Integrating outcrop and subsurface data to assess the temporal evolution of a submarine channel–levee system

Emma A. Morris, David M. Hodgson, Stephen Flint, Rufus L. Brunt, Stefan M. Luthi, and Yolanda Kolenberg

ABSTRACT

The morphological evolution of submarine channel systems can be documented using high-resolution three-dimensional seismic data sets. However, these studies provide limited information on the distribution of sedimentary facies within channel fills, channel-scale stacking patterns, or the detailed stratigraphic relationship with adjacent levee-overbank deposits. Seismic-scale outcrops of unit C2 in the Permian Fort Brown Formation, Karoo Basin, South Africa, on two subparallel fold limbs comprise thin-bedded successions, interpreted as external levee deposits, which are adjacent to channel complexes, with constituent channels filled with thick-bedded structureless sandstones, thinner-bedded channel margin facies, and internal levee deposits. Research boreholes intersect all these deposits, to link sedimentary facies and channel stacking patterns identified in core and on image logs and detailed outcrop correlation panels. Key characteristics, including depth of erosion, stacking patterns, and cross-cutting relationships, have been constrained, allowing paleogeographic reconstruction of six channel complexes in a 36-km^2 (14-mi^2) area. The system evolved from an early, deeply incised channel complex, through a series of external levee-confined and laterally stepping channel complexes culminating in an aggradational channel complex confined by both internal and external levees. Down-dip divergence of six channel complexes from the same location suggests the presence of a unique example of an exhumed deep-water avulsion node. Down-dip, external levees are supplied by flows that escaped from channel complexes of different ages and spatial positions and are partly confined and share affinities with internal levee successions. The absence of frontal lobes suggests that the channels remained in sand bypass mode immediately after avulsion.

Manuscript received March 29, 2015; provisional acceptance September 10, 2015; revised manuscript received March 5, 2016; final acceptance April 27, 2016.
DOI:10.1306/04271615056

AUTHORS

EMMA A. MORRIS ~ *Stratigraphy Group, Geology and Geophysics, School of Environmental Science, University of Liverpool, 4 Brownlow Street, Liverpool, L69 3GP United Kingdom; present address: Badley Ashton America Inc., 14701 St Mary's Lane, Ashford 5, Suite 375, Houston, Texas 77079; eramorris@outlook.com*

Emma A. Morris received a B.Sc. in geoscience from the University of St. Andrews (2009) and completed a Ph.D. (2014) at the University of Liverpool on the characterization of deep-water channel–levee systems. She is currently at Badley Ashton (Houston), where she specializes in the sedimentology and architecture of deep-water systems, with a focus on Paleogene deposits in the Gulf of Mexico.

DAVID M. HODGSON ~ *Stratigraphy Group, School of Earth and Environment, University of Leeds, Leeds, LS2 9JT United Kingdom; d.hodgson@leeds.ac.uk*

David M. Hodgson received a B.Sc. (1996) in geology and physical geography from the University of Liverpool and a Ph.D. (2002) from University College London. He is professor of sedimentology and stratigraphy at the University of Leeds. His research focus is the stratigraphic record of sedimentary basins, and he is co–principal investigator for the Lobe2 and Slope4 Joint Industry Programs.

STEPHEN FLINT ~ *Stratigraphy Group, School of Earth, Atmospheric and Environmental Sciences, University of Manchester, Oxford Road, Manchester, M13 9PL United Kingdom; stephen.flint@manchester.ac.uk*

Stephen Flint received a Ph.D. from the University of Leeds in 1985 and joined Shell Research in Rijswijk (The Netherlands). In 1989 he moved to the University of Liverpool, where he founded the Stratigraphy Group. He gained a full professorship in 1998 and moved to the University of Manchester in 2012. Research interests include deep-water architecture and hierarchies in stratigraphy.

RUFUS L. BRUNT ~ *Stratigraphy Group, School of Earth, Atmospheric and*

Environmental Sciences, University of Manchester, Oxford Road, Manchester, M13 9PL United Kingdom; rufus.brunt@manchester.ac.uk

Rufus L. Brunt attended the University of Leeds, graduating with a B.Sc. in geology and physical geography (1996) and a Ph.D. (2004). He is currently a lecturer in petroleum geology at the University of Manchester, where his research interests include clastic sedimentology and stratigraphy.

Stefan M. Luthi ~ *Department of Geoscience and Engineering, Delft University of Technology, Stevinweg 1, 2628 CN Delft, The Netherlands; s.m.luthi@tudelft.nl*

Stefan M. Luthi received an M.Sc. and a Ph.D. in geology from Eidgenössische Technische Hochschule Zurich, Zurich (Switzerland). He joined Schlumberger in 1982 and moved to Delft University of Technology (The Netherlands) in 1999, where he is currently professor emeritus in production geology. He has authored over 50 peer-reviewed publications and the book *Geological Well Logs–Their Use in Reservoir Modeling*.

Yolanda Kolenberg ~ *Department of Geoscience and Engineering, Delft University of Technology, Stevinweg 1, 2628 CN Delft, The Netherlands; yolanda.kolenberg@shell.com*

Yolanda Kolenberg received a B.Sc. (2008) in applied earth sciences and an M.Sc. (2011) in petroleum engineering and reservoir geology from Delft University of Technology, The Netherlands. Yolanda works as a well engineer for Nederlandse Aardolie Maatschappij/Shell and is involved in both drilling operations and well design. She previously worked in the solution salt mining industry, studying cavern shapes and the Zechstein salt flow.

ACKNOWLEDGMENTS

The authors gratefully acknowledge the local farmers for fieldwork access and De Ville Wickens for logistical support and management of well site geology and drilling operations. Ashley Clarke, Miquel Poyatos-Moré, Giuseppe Malgesini, John Kavanagh, and Koen Van Toorenenburg are acknowledged for fieldwork support. Laura

INTRODUCTION

Submarine channel–levee systems are a primary conduit for clastic sediment supplied from the continents to the deep ocean (Shepard and Emery, 1941; Shepard, 1948, 1981; Menard, 1955; Normark, 1970; Normark and Carson, 2003; Kolla, 2007; Normark et al., 2009; Peakall and Sumner, 2015). The architecture and evolution of deep-water channel systems has been of particular interest in both the hydrocarbon industry and academic study in recent years with detailed investigations using high-resolution reflection seismic data sets (e.g., McHargue and Webb, 1986; Badalini et al., 2000; Babonneau et al., 2002, 2004; Abreu et al., 2003; Deptuck et al., 2003, 2007; Posamentier, 2003; Posamentier and Kolla, 2003; Schwenk et al., 2005; Mayall et al., 2006; Kolla, 2007; Cross et al., 2009; Catterall et al., 2010; Armitage et al., 2012; Jobe et al., 2015; Ortiz-Karpf et al., 2015) and seabed imaging techniques (e.g., Torres et al., 1997; Maier et al., 2011, 2013; Covault et al., 2014), although these provide limited detailed information on subseismic-scale elements and the range and distribution of sedimentary facies. This gap has been addressed through the use of analogous systems at outcrops (Badescu et al., 2000; Blikeng and Fugelli, 2000; Campion et al., 2000; Clark and Gardiner, 2000; Gardner et al., 2003; Beaubouef, 2004; Pickering and Corregidor, 2005; Hodgson et al., 2011; Brunt et al., 2013b; Hubbard et al., 2014; Masalimova et al., 2016). Although these studies help to constrain the distribution and lateral variation of sedimentary facies of channel fills, channel-scale stacking patterns, and detailed stratigraphic relationship with adjacent levee-overbank deposits, they typically have limited three-dimensional (3-D) control or calibration with subsurface data sets. Rare examples of outcrop-based studies with subsurface constraint of channelized systems include the Eocene of the Ainsa Basin, northeast Spain (e.g., Pickering and Corregidor, 2005); the Miocene Mount Messenger Formation, New Zealand (Browne and Slatt, 2002); and the Permian Brushy Canyon Formation, United States (Beaubouef et al., 1999). Outcrop studies where slope channel systems can be traced in multiple outcrop exposures providing 3-D constraint are also rare (Hubbard et al., 2008; Pyles et al., 2010; Macauley and Hubbard, 2013).

Many studies have documented the highly organized nature of deep-water deposits, suggesting a regular, ordered set of controls on the development of stratal architecture (e.g., Beaubouef et al., 1999; Gardner et al., 2003; Hodgson et al., 2006, 2011, 2016; Pyles, 2008; Flint et al., 2011; Terlaky et al., 2016). This stratigraphic organization has enabled the development of a hierarchical approach to both confined and unconfined parts of deep-water systems. For channelized sections, Sprague et al. (2002) developed a hierarchy of stories and story sets that build channels.

Channels stack into channel complexes and channel complex sets (McHargue et al., 2011). These hierarchical schemes bridge the scale between well data and the vertical resolution of industry seismic reflection surveys, in which the smallest resolvable element is typically the complex or complex set.

In this paper, we present a combined outcrop and subsurface study of a channel–levee complex set and the sedimentary facies distribution and depositional architecture of six constituent channel complexes. The succession is part of unit C of the Fort Brown Formation, Laingsburg Karoo Basin, South Africa (Figure 1). Six research boreholes (named Bav 1a–Bav 6) drilled behind the outcrop intersect channel axis, channel margin, internal levee, and external levee deposits. These provide detailed information on sedimentary facies and channel-stacking patterns identified in one-dimensional (1-D) core, gamma-ray, and borehole image logs that are integrated with two detailed across-depositional strike two-dimensional (2-D) correlation panels from adjacent outcrop (Hodgson et al., 2011; Kane and Hodgson, 2011). These data are integrated to produce highly detailed paleogeographic reconstructions at subseismic resolution to argue for the presence of unique examples of an exhumed deep-water avulsion node and confined external levee deposits.

GEOLOGIC SETTING AND STRATIGRAPHY

The study area forms part of the Permian deep-water Laingsburg depocenter of the southwestern Karoo Basin (Figure 1). A long-standing interpretation for the formation of the Karoo Basin is that it represents a retroarc foreland basin formed through flexural loading from the adjacent fold-thrust belt (Cape fold belt) lying along the southern margin of the basin (De Wit and Ransome, 1992; Veevers et al., 1994; Visser and Praekelt, 1996; Catuneanu et al., 1998). In a more recent synthesis of published data with a recent seismic refraction survey, Tankard et al. (2009) proposed that the Cape fold belt is Triassic in age and interpreted Karoo Basin subsidence as caused by mantle flow associated with subduction-related by negative dynamic topography but complicated by variable degrees of foundering of basement blocks.

A 1-km-thick (4600-ft-thick) exhumed progradational basin floor to upper slope succession (Flint et al., 2011; van der Merwe et al., 2014) crops out along a series of east–west-trending, eastward plunging, postdepositional anticlines and synclines, near the town of Laingsburg (Figures 1, 2). Deep-water deposition began with distal basin floor deposits of the Vischkuil Formation (van der Merwe et al., 2009, 2010), which is overlain by basin floor and base-of-slope fan systems of the Laingsburg Formation (units A and B; Grecula et al., 2003; Sixsmith et al., 2004). The muddy slope succession of the 0.5-km-thick (1640-ft-thick)

Fielding, Amandine Prélat, William Palmer, and Andrew Adamson are acknowledged for their support during core logging, and we thank the Council for Geosciences, Pretoria, for their kind support in core preparation, storage, and use of facilities. The SLOPE Phase 3 Project consortia sponsors (Anadarko, BHPBilliton, BP, Chevron, ConocoPhillips, E.ON, ExxonMobil, Engie, Maersk, Murphy, nce Suez, Nexen, Petrobras, Schlumberger, Shell, Statoil, Total, Tullow, VNG Norge, and Woodside) are acknowledged for financial support and for important technical feedback. We would also like to thank reviewers Andrea Fildani and Kirt Campion for their thorough and constructive reviews.

DATASHARE 75

Tables A–F are available in an electronic version on the AAPG website (www.aapg.org/datashare) as Datashare 75.

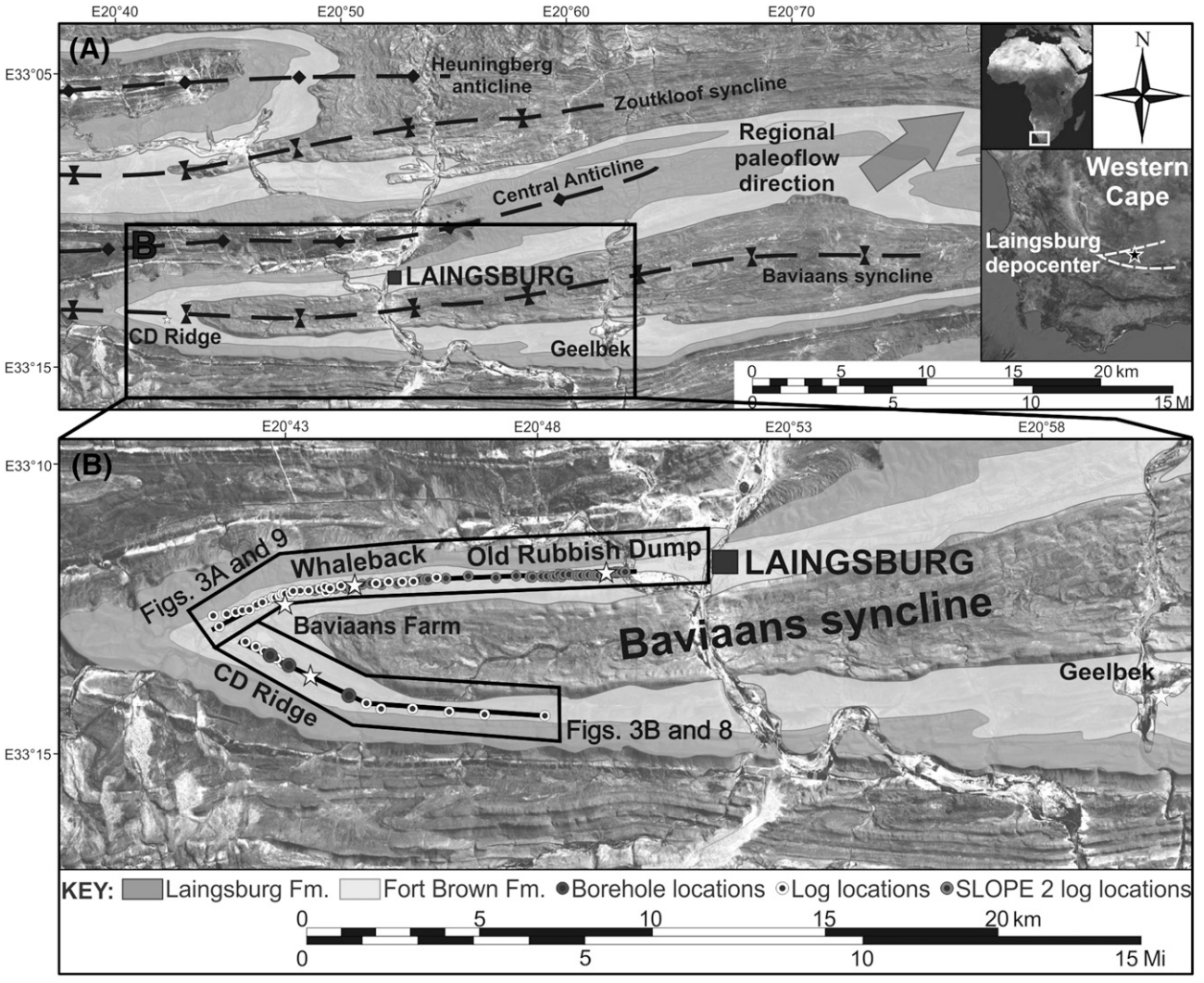

Figure 1. Location map highlighting the study area near the town of Laingsburg, Western Cape, South Africa. The pale gray area marks the outcrops of the Laingsburg Formation (Fm.), and dark gray shows the outcrop pattern of the Fort Brown Formation. SLOPE 2 refers to a previous research consortium project.

overlying Fort Brown Formation (Figure 2) is punctuated by five sandstone-rich units (units C–G; Flint et al., 2011) that comprise slope channel–levee systems separated vertically by extensive mudstone units (Grecula et al., 2003; Figueiredo et al., 2010; Di Celma et al., 2011; Hodgson et al., 2011; Morris et al., 2014a). These mudstone units constrain the stratigraphy and have been mapped for up to 90 km (56 mi) downdip (van der Merwe et al., 2014). In this study, the focus is on unit C, primarily exposed in the Baviaans syncline (Figure 1). Regional paleoflow is toward the northeast (Di Celma et al., 2011).

Unit C overlies the B–C mudstone, an approximately 50-m-thick (164-ft-thick) partly hemipelagic drape that separates the Laingsburg and Fort Brown Formations (Figure 2). This mudstone contains a less than 5-m-thick (<16-ft-thick), sharp-topped and sharp-based sandstone-dominated unit referred to as the B–C interfan (Figure 2B) (Di Celma et al., 2011), interpreted by Flint et al. (2011) as an intraslope lobe. It lies approximately 32 m (108 ft) below the base of unit C, and it is used as a lower datum when measuring and correlating units C and D.

Unit C has been interpreted as the lowstand sequence set (LSS) to a composite sequence, the combined transgressive and highstand sequence set of which is represented by the approximately 26-m-thick (85-ft-thick) regional C–D mudstone (Flint et al., 2011). The unit C LSS comprises three sequences; their lowstand systems tracts are sandy

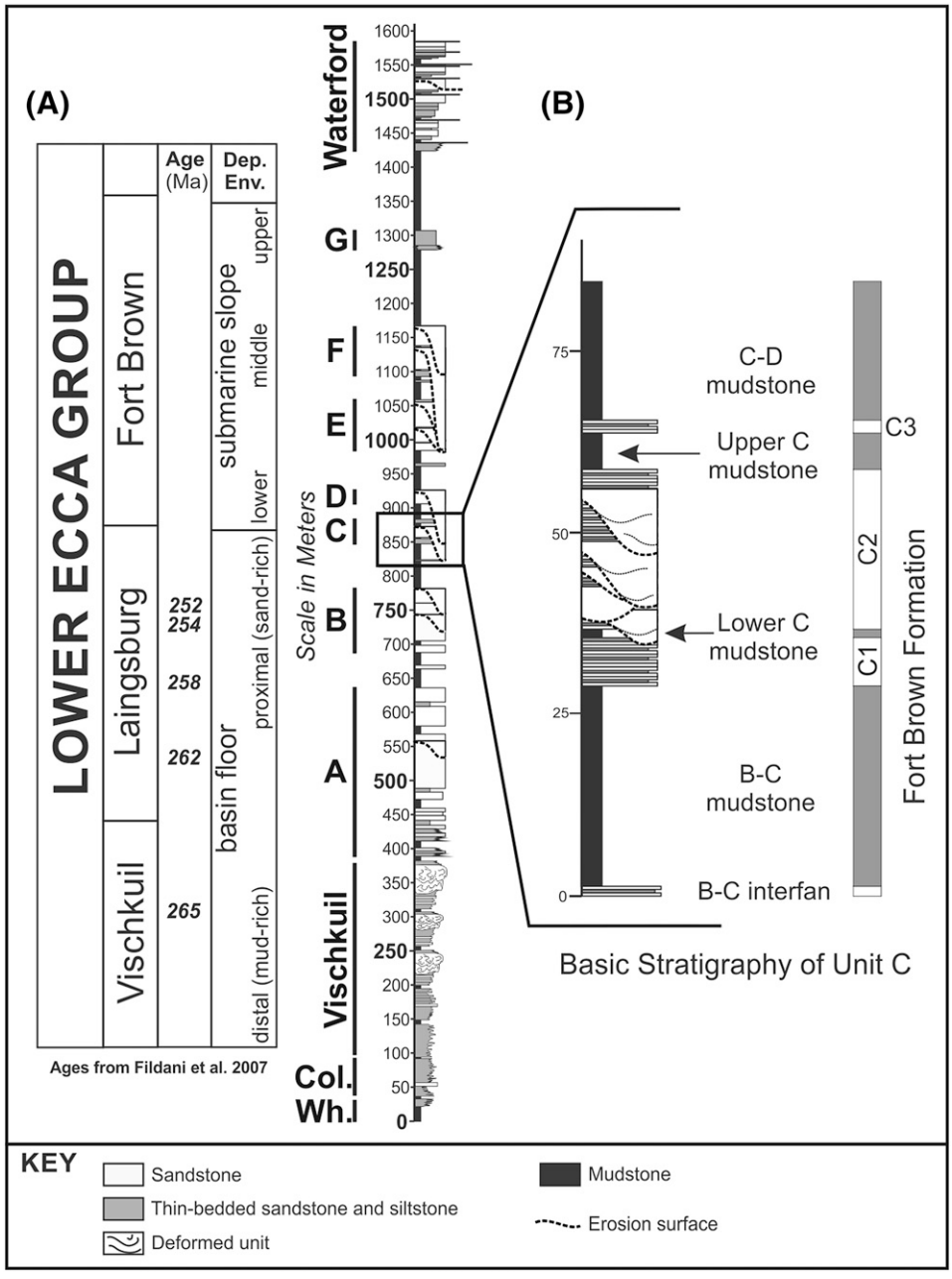

Figure 2. (A) Stratigraphic column showing the lithostratigraphy of the study area. (B) Expanded stratigraphic column highlighting unit C, the focus of this study. Col. = Collingham Formation; Dep. Env. = depositional environment; Wh. = Whitehill Formation.

subunits C1, C2, and C3 (Di Celma et al., 2011; Flint et al., 2011). These are separated by two intraunit mudstones; a 2-m-thick (6.5-ft-thick) lower C mudstone and an approximately 8-m-thick (26-ft-thick) upper C mudstone (Figure 2). Both have been mapped regionally and have been interpreted as the combined transgressive systems tracts–highstand systems tracts (TST–HST) of the C1 and C2 sequences. The TST–HST of the C3 sequence is the lower part of the C–D mudstone (Flint et al., 2011). In the Baviaans area, subunit C1 is generally 10- to 15-m-thick (33- to 49-ft-thick) and composed of sandstone-prone thin beds becoming more siltstone-prone upward; it has been interpreted as a frontal lobe complex (Di Celma et al., 2011). Subunit C2 is 5- to 80-m-thick (16- to 260-ft-thick) and largely comprises thin-bedded sandstones and siltstones interpreted as external levee deposits that are adjacent to channels filled with thick-bedded structureless channel axial sandstone (Morris et al., 2014a), thin-bedded channel margin material (Hodgson et al., 2011), and thin-bedded internal levee deposits (Kane and Hodgson, 2011) (Figure 3). The thickest accumulations are a result of erosive channelization in proximal areas,

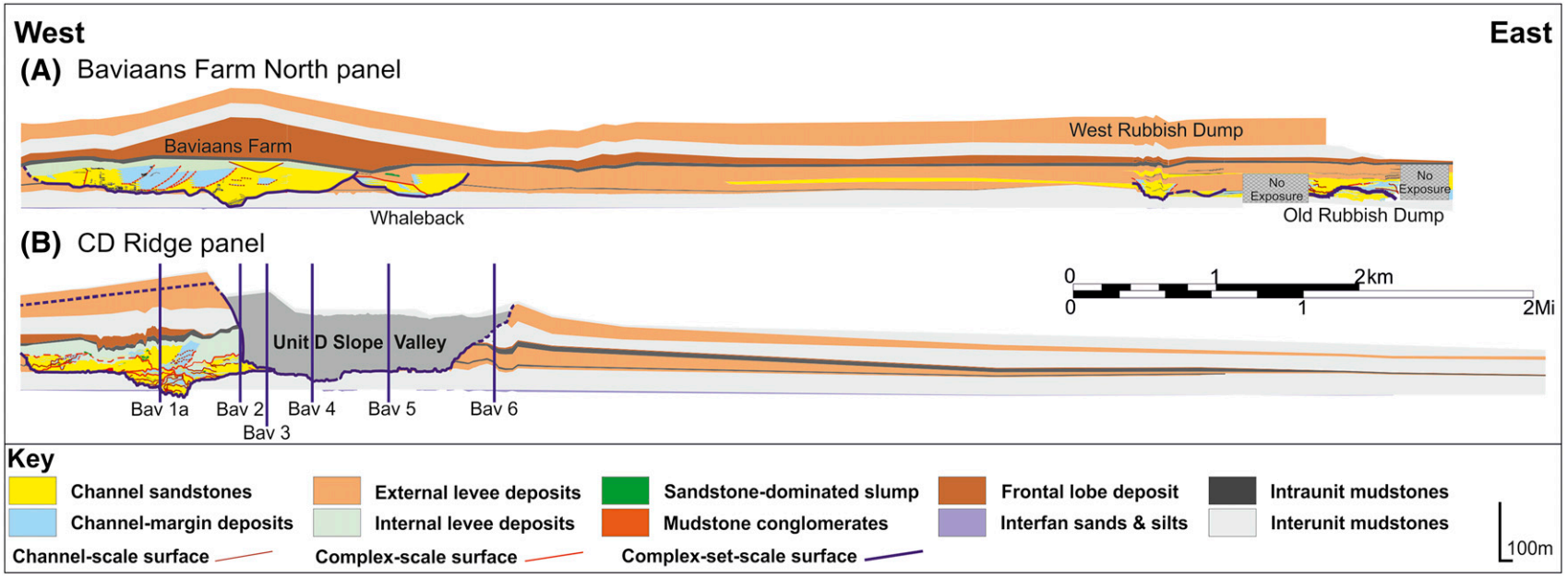

Figure 3. (A) Correlation panel of units C and D on the north limb of the Baviaans syncline showing the main channel complexes at Baviaans Farm, the Whaleback, the West Rubbish Dump, and the Old Rubbish Dump. (B) Correlation panel of units C and D on the south limb of the Baviaans syncline at the CD Ridge. The unit D slope valley that incises through the entire unit C stratigraphy has been blanked out in gray. The locations of all six behind-outcrop boreholes are represented by vertical lines. Boreholes Bav 1a (Figure 4) and Bav 2 (Figure 5) are incorporated in this study.

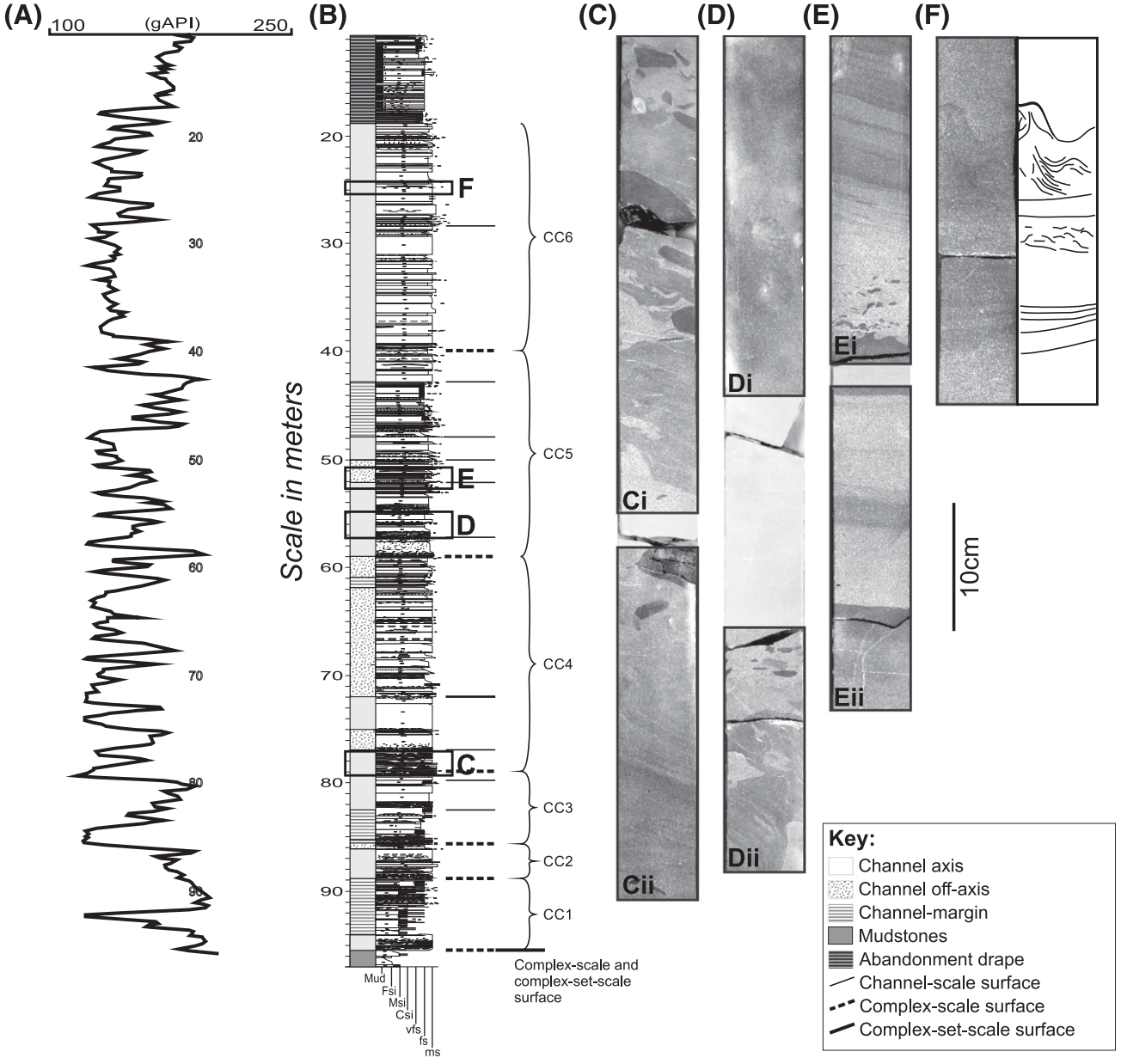

Figure 4. (A) Gamma-ray log through subunit C2 in borehole Bav 1a. (B) Core log through C2 in borehole Bav 1a. Boxed areas C–F give positions of core photographs in (C)–(F): (C) Photo Ci is a core photo showing different clast compositions at the base of a channel complex, and photo Cii shows soft sediment deformation. (D) Photo Di shows structureless fine-grained sandstone, and photo Dii shows soft sediment deformation within siltstone and sandstone clasts. (E) Photo Ei shows fine-grained sandstone with a well-developed loaded basal surface with mudstone clasts, and photo Eii shows planar laminated sandstone with normal grading. (F) Structureless fine-grained sandstone with a well-developed flame structure. CC1 = channel complex 1; CC2 = channel complex 2; CC3 = channel complex 3; CC4 = channel complex 4; CC5 = channel complex 5; CC6 = channel complex 6; Csi = coarse-grained siltstone; Fsi = fine-grained siltstone; fs = fine-grained sandstone; ms = medium-grained sandstone; Msi = medium-grained siltstone; Mud = mud grade sediment; vfs = very fine-grained siltstone.

where C2 comprises a levee-confined channelized system that incises through C1 and 30 m (98 ft) of the underlying mudstone (Hodgson et al., 2011).

Subunit C3 is commonly 1–10 m (3–33 ft) thick, attains a maximum thickness of greater than 50 m (164 ft) in the proximal Baviaans area, and is interpreted as a frontal lobe complex (Morris et al., 2014b). Di Celma et al. (2011) described a progradational trend from subunit C1 to C2, with a landward stepping (retrogradational) component during the deposition of C3, suggesting a waxing then waning of overall sediment supply during the unit C

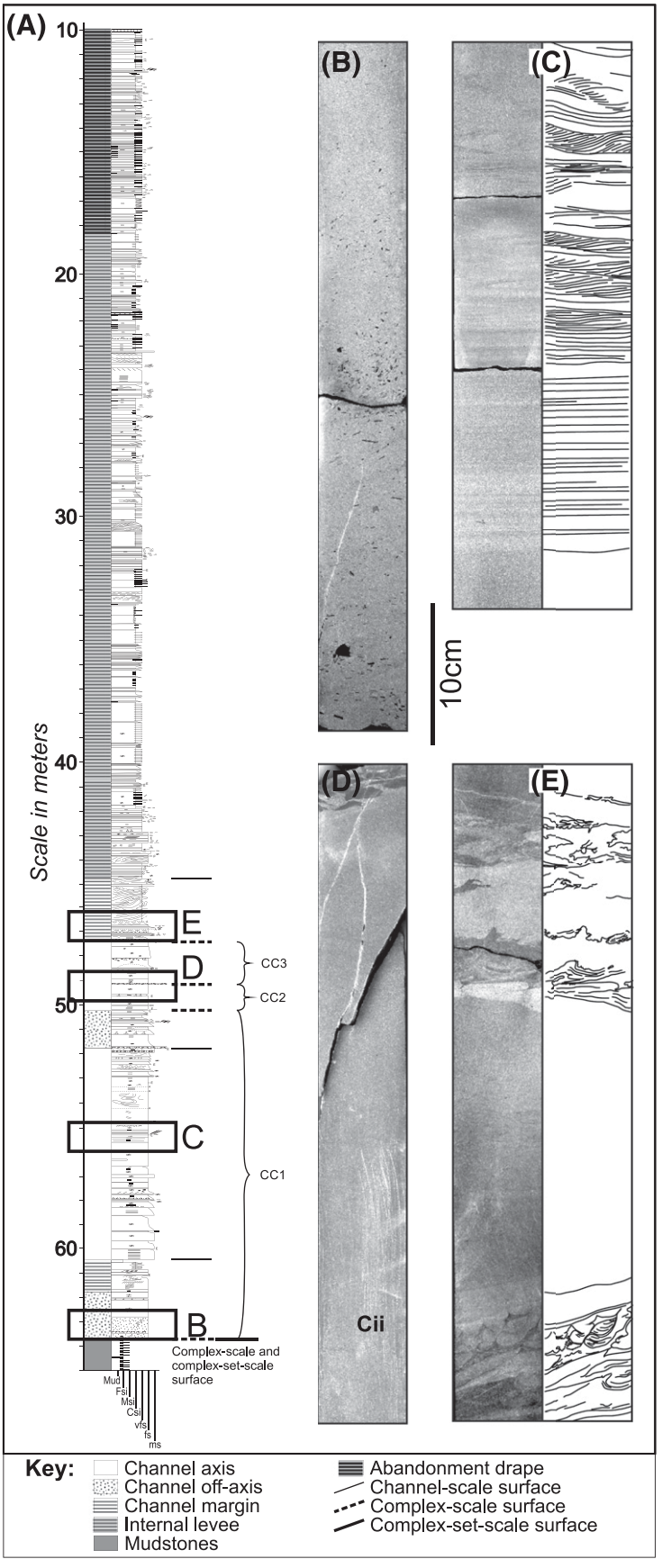

Figure 5. (A) Core log through subunit C2 in borehole Bav 2. (B) Fine-grained sandstone with mudstone clasts dispersed throughout the entire 1-m (3-ft) section (location of core photograph shown on core log A). (C) Core photograph and interpretation showing an upward progression from structureless fine-grained sandstone to planar lamination followed by climbing ripple lamination. (D) Structureless fine sandstone with a mudclast mantled channel base at the top of the core interval. (E) Deformed and dewatered fine-grained sandstone showing a well-developed loaded basal contact and an upper deformed sandstone and siltstone zone. CC1 = channel complex 1; CC2 = channel complex 2; CC3 = channel complex 3; Csi = coarse-grained siltstone; fs = fine-grained sandstone; Fsi = fine-grained siltstone; ms = medium-grained sandstone; Msi = medium-grained siltstone; Mud = mud grade sediment; vfs = very fine-grained siltstone.

lowstand sequence set. Unit D, interpreted as another lowstand sequence set (Flint et al., 2011), crops out as a 2-km-wide (1-mi-wide), greater than 100-m-thick (330-ft-thick), entrenched slope valley fill at the CD Ridge (Figures 2, 3) on the south limb of the Baviaans syncline where it removes part of unit C (see Hodgson et al., 2011, for further details).

METHODOLOGY AND DATA SET

The primary study area covers 36 km^2 (14 mi^2) in which units C and D crop out on the north and south limbs of the Baviaans syncline (Figure 1). Correlation panels constructed on both limbs of the structure (Figure 3) capture the evolving style of channels and levees in C2. Field-based sedimentological and stratigraphic observations including 247 measured sections (16 km [10 mi] of cumulative thickness) were used to construct the correlation panels: 147 sections for the panel on the north limb of the Baviaans syncline (Pringle et al., 2010; Di Celma et al., 2011) and 100 sections in the western area of the CD Ridge panel on the south limb of the syncline (Di Celma et al., 2011; Hodgson et al., 2011). Channelized deposits within C2 have been described in detail from two of the research boreholes, Bav 1a (Figure 4) and Bav 2 (Figure 5), and external levee deposits in Bav 6 (Morris et al., 2014a). A suite of slim-hole well logs was collected that include borehole electrical images with the formation microscanner (FMS) tool (Mark of Schlumberger). These images are orientated with respect to geographic north, and therefore, the direction of paleocurrent indicators was determined. No logs were run in the Bav 2 well because of a loss of the drill bit in the hole. The combination of well-constrained outcrop data on the south and north limbs of the Baviaans syncline (Figure 3) and continuous core in the three boreholes that intersect the C2 system permits a high-confidence understanding of what can be recognized from combinations of conventional wireline and borehole image logs. The porosities, permeabilities, and fluid saturations of the rocks, however, are not comparable to oil or gas reservoirs because the Karoo Basin deposits have been buried to depths greater than 6 km (>4 mi) and are highly compacted and cemented by quartz. Detrital clay minerals have been transformed into low-grade metamorphic minerals (Luthi et al., 2006). As a result, density and neutron porosity logs were not run, and conventional logging was restricted to spectral gamma-ray and sonic logs.

FACIES ASSOCIATIONS

In the channelized C2 succession, six facies associations have been identified and are shown in Table 1: CLf1 is a thick-bedded, structureless fine-grained sandstone; CLf2 is structureless fine-grained sandstone with mudstone and siltstone clasts; CLf3 is structured fine- and very fine–grained sandstone; CLf4 is sand-prone thin beds; CLf5 is silt-prone thin beds; and CLf6 is deformed heterolithic sediments. Subunit C2 has been well documented in outcrop (Di Celma et al., 2011; Hodgson et al., 2011) and in core from adjacent boreholes in this study. Six main environments of deposition have been interpreted: (1) channel axis (CLf1 and CLf2), (2) channel margin (CLf3, CLf4, CLf5, and CLf6), (3) proximal internal levee (CLf3 and CLf4), (4) distal internal levee (CLf4), (5) proximal external levee (CLf3, CLf4, and CLf5), and (6) distal external levee (CLf4 and CLf6). Table 2 shows key facies examples from the combined outcrop, core, and borehole image data sets for each of the environments of deposition.

ONE-DIMENSIONAL DATA SET: BEHIND OUTCROP CORES AND WIRELINE LOGS

Of the six research boreholes drilled behind the CD Ridge, three (Bav 1a, Bav 2, and Bav 6) intersected C2. Boreholes Bav 1a and Bav 2 are approximately 0.7 km (0.44 mi) apart (Figure 3), whereas Bav 6 is situated approximately 2 km (1 mi) east of Bav 2. Borehole Bav 1a captures the C2 axis where it has locally removed the B–C interfan, Bav 2 captures a more eastward component of the channel complex set and part of the unit D slope valley, and Bav 6 intersects the external levee of C2 (Kane and Hodgson, 2011; Morris et al., 2014a) (Table 2).

Borehole Bav 1a

In Bav 1a, six channel complexes (channel complex 1 [CC1]–channel complex 6 [CC6]) have been interpreted (Figure 4). Fine-grained sandstone with multiple erosion surfaces lined by mudstone and siltstone

Table 1. Characteristics of the Six Facies Associations of Subunit C2

Lithofacies Code	Facies	Facies Description	Depositional Processes and Depositional Environments
CLf1	Thick-bedded, structureless fine-grained sandstone	Thick-bedded fine-grained sandstone bedsets 0.1–2 m (0.33–6.56 ft), commonly thicker than 0.3 m (0.98 ft). Amalgamated bed contacts are most prevalent; however, erosive and loaded bed bases are recorded. Sandstone beds are generally structureless; however, rare occurrences of planar and current ripple lamination are observed, and thicker beds commonly contain abundant water escape structures, commonly flame and dish structures. A general trend exists of individual beds grading normally upward.	Medium- to high-density flows depositing rapidly. Aggradational facies, amalgamated sandstone deposits with some erosion surfaces. Structureless sandstone bedsets suggest Bouma T_a. Environment of deposition: Fall in capacity of high-concentration flows and rapid deposition. Late-stage fill within channels and proximal areas of frontal lobes.
CLf2	Structureless fine-grained sandstone with mudstone and siltstone clasts	Structureless fine-grained sandstone beds, approximately 0.25–0.7 m (0.82–2 ft) thick, reaching up to 1 m (4 ft). Mudstone clasts are abundant, averaging between less than 0.01 and 0.04 m (0.03 and 0.13 ft) in diameter, although some are approximately 0.2 m (0.66 ft) in diameter. Rare examples of thin horizons (0.01–0.05 m [0.03–0.16 ft]) where a slurry of sandstone with abundant millimeter-sized mudstone clasts is present. The mudclast-rich zone is generally preserved at/near the base of sand units, and the clasts themselves become sandier in composition up through the succession of subunit C2 (this is best observed in core Bav 1a).	Mudstone clast mantled surfaces and mudclast conglomerate deposited and moved in traction beneath confined flows. They are both commonly associated with flows confined within channels. Locally, clasts show secondary injection features. Environment of deposition: The presence of mudstone clasts indicates erosion higher in the channel profile. Mudstone clasts are deposited as a channel lag/drape.
CLf3	Structured sandstones	Very fine–grained sandstone beds (VFS) 0.05–0.4 m (0.16–1 ft) thick. Well-developed current ripple cross-lamination, climbing ripple (10–15°) cross-lamination, stoss-side preserved ripple cross-lamination, and sinusoidal laminae are common. Small-scale (centimeter–decimeter) erosion surfaces, some soft-sedimentary deformation, but little bioturbation and few mudstone drapes present. Overall, there is little silt or clay grade material present. Individual beds continuous for greater than 100 m (328 ft).	Rapidly deposited medium- to low-density turbidity currents. Aggradational facies, with some erosion surfaces. Sustained bedload traction, particularly within or close to channels. Environment of deposition: Deposition from expanding flows with sustained bedload traction: frontal lobe, crevasse splay, internal levee, and/or proximal external levee.

(*continued*)

Table 1. Continued

Lithofacies Code	Facies	Facies Description	Depositional Processes and Depositional Environments
CLf4	Sand-prone thin-bedded heterolithics	Sandstone-dominated interbedded sandstone and siltstone packages 0.05–0.4 m (0.16–1 ft) thick. The sandstone beds are generally normally graded from VFS to coarse siltstone (CSi). Sedimentary structures within the VFS beds include sinusoidal laminae, current ripple cross-lamination, climbing ripple cross-lamination, stoss-side preserved ripple cross-lamination, and planar laminae. The CSi beds are generally planar laminated. Loaded bed contacts are common, although erosive and amalgamated basal contacts are observed.	Deposition by low- to medium-density turbidity currents that deposited rapidly (climbing ripple cross-lamination and sinusoidal lamination). Environments of deposition: This facies is present in channel margin, proximal internal levee, and proximal external levee subenvironments.
CLf5	Silt-prone thin-bedded heterolithics	Interbedded CSi and VFS, beds are 0.01–0.3 m (0.03–0.98 ft) thick. VFS beds are commonly normally graded. Sedimentary structures present in the VFS include current ripple lamination, stoss-side preserved ripple lamination, wavy lamination, and planar lamination. The CSi beds are commonly planar laminated and are generally interbedded with mudstone drapes associated with bioturbation.	The bed thicknesses and the low sand volume suggest that deposition was by dilute turbidity currents. The bioturbated interval suggests either there was a longer time period between events or a change in oxygen and nutrient delivery. Environment of deposition: Regions distal to sediment feeder system, such as distal overbank, distal levee (internal and external examples), channel margin, distal lobe, or abandonment.
CLf6	Deformed heterolithics	Highly deformed bedded lobe to channel sandstone deposits. All predeformed textures and structures are still recognized, and deformed material can be traced back into predeformed deposits. Where present, gentle folding of grain laminations or bed surfaces suggests small transport distances. Internal characteristics not easily identified in structureless sandstones. Packages are generally less than 2 m (7 ft) thick; however, the deposit may extend for up to 100 m (328 ft) across outcrop.	A loss of internal shear strength in all or part of a sediment mass resulting in a failure where the deposit can no longer resist downslope gravitational shear occurs on a large scale with slope margin collapse and on a small scale as slumping and sliding at the steepened margins of channels. Environment of deposition: Fill within erosional channels (channel wall collapse). Normally associated with the collapse of deeply erosional and oversteepened incisional margins.

clasts (Figure 4C) (CLf2), typical of channel axis and channel off-axis environments, produce an erratic gamma-ray log trace. Packages of structureless fine-grained sandstone between the erosion surfaces show dewatering features (CLf1) (Figure 4). The composition of the clasts changes upward through the succession, from mudstone- to siltstone- and sandstone-dominant. Many of the clast-lined erosion surfaces are spaced at 1–2 m (3–7 ft) vertically. Without the control from the nearby outcrop it would be easy to consider these units as too thin for channels and to therefore interpret them as story boundaries. However, the detailed outcrop logs, spaced at 20-m (66-ft) intervals along the CD Ridge, where every bed

Table 2. The Six Main Environments of Deposition Interpreted within C2

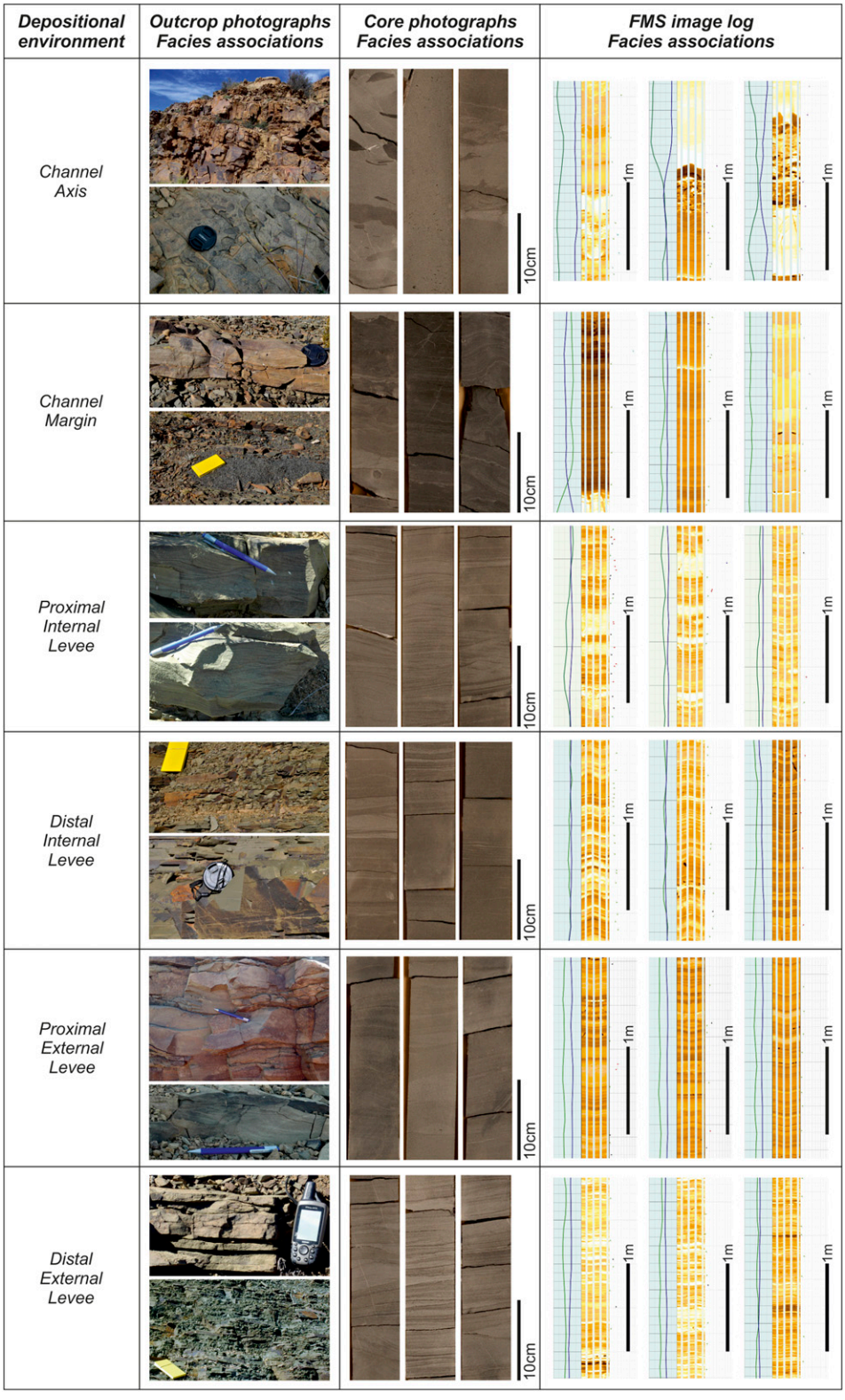

See Tables A–F (supplementary material available as AAPG Datashare 75 at www.aapg.org/datashare) for more details. FMS = formation microscanner.

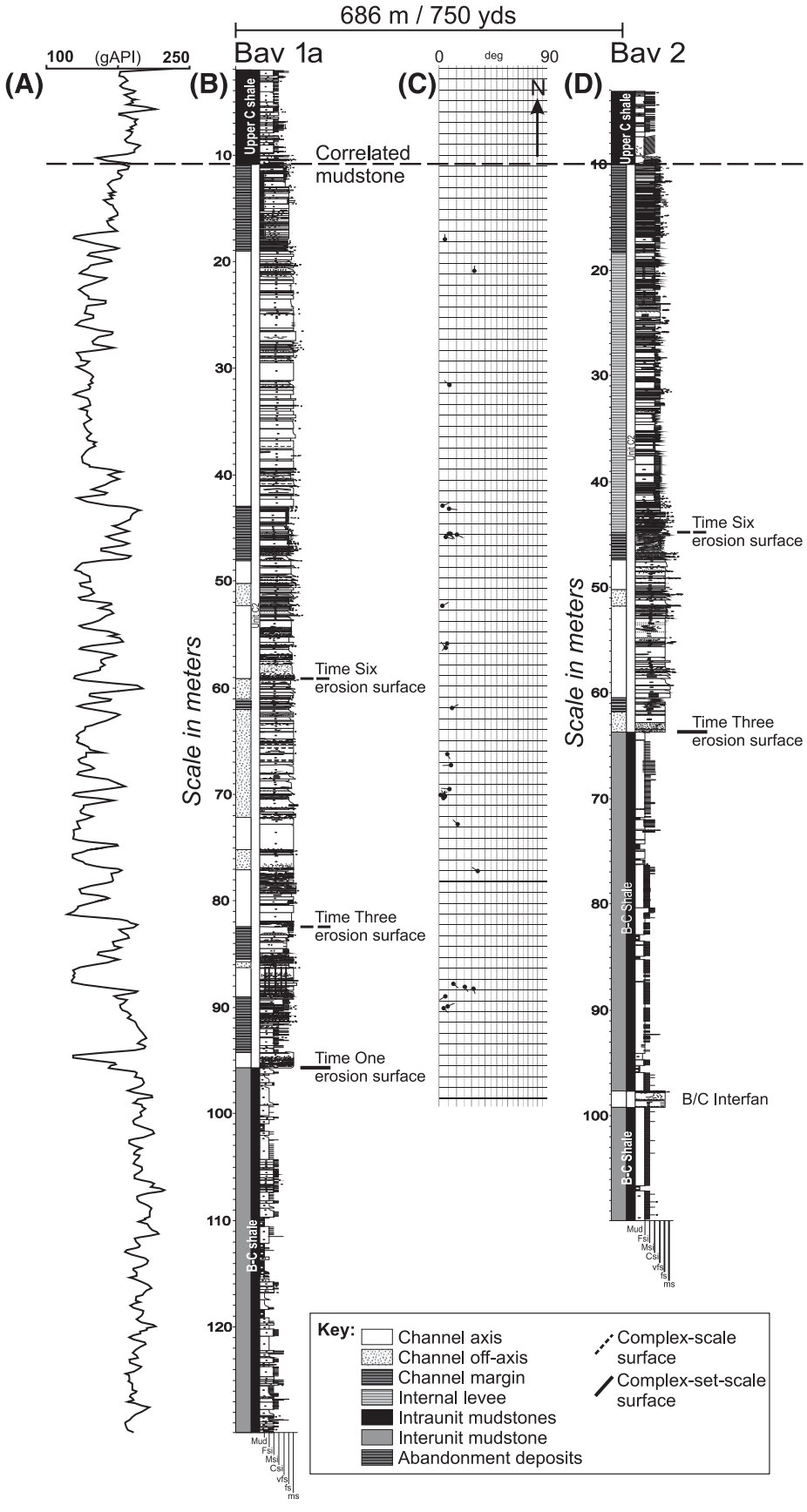

Figure 6. Correlation panel between boreholes Bav 1a and Bav 2 using the Upper C mudstone as a datum: (A) Gamma-ray log through Bav 1a;. (B) Bav 1a sedimentary log (no well logs were run in this borehole). (C) Dipmeter measurements of erosion surfaces in subunit C2. (D) Bav 2 sedimentary log. Csi = coarse-grained siltstone; fs = fine-grained sandstone; Fsi = fine-grained siltstone; ms = medium-grained sandstone; Msi = medium-grained siltstone; Mud = mud grade sediment; vfs = very fine-grained siltstone.

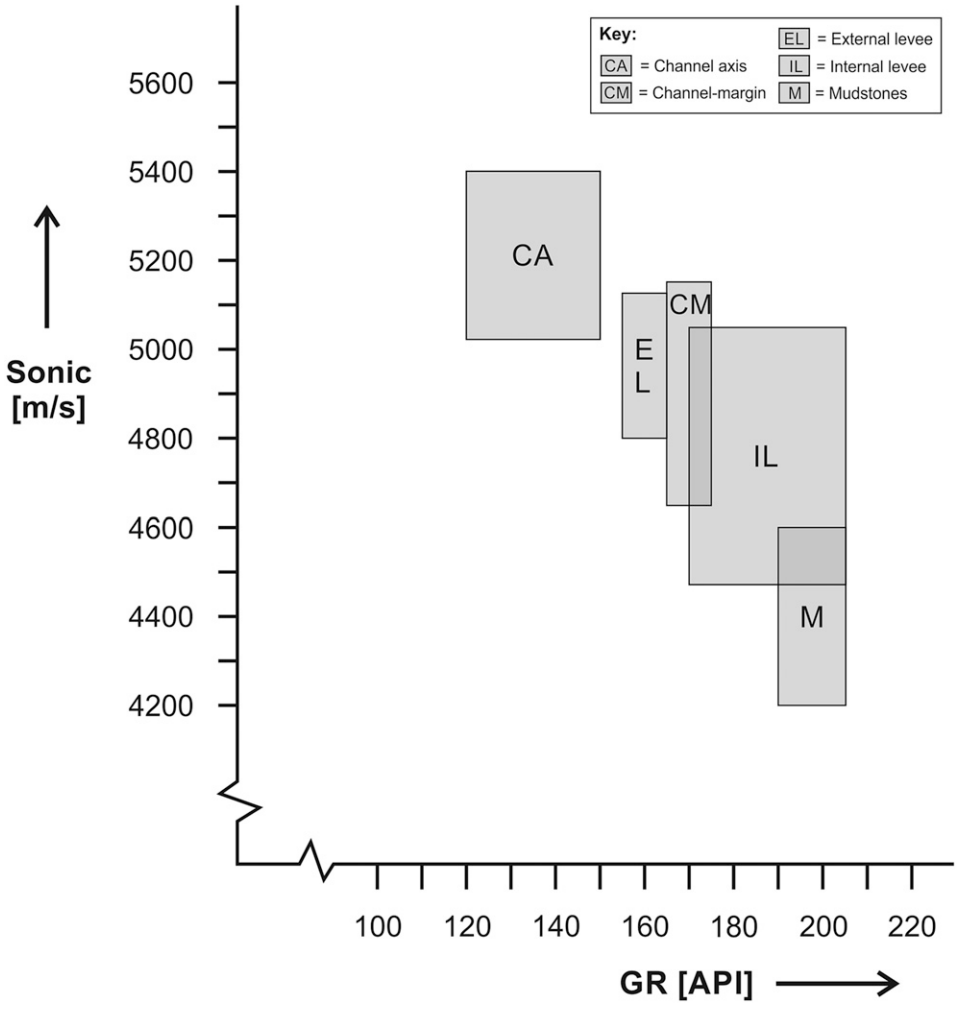

Figure 7. Cross-plot of gamma-ray (GR) and sonic log values, exhibiting typical ranges for the main architectural elements of the unit C depositional system.

has been traced between them (Hodgson et al., 2011), show that the lower part of C2 is composed of stacked erosional remnants of channel fills. Distinction of a channel base from a channel complex base is informed by outcrop observations, and the bases of channel complexes are marked by thicker concentrations of mudstone and siltstone rip-up clasts, which are interpreted as lag deposits that mark time periods dominated by sediment bypass (Stevenson et al., 2015). Thickness increases upward between erosion surfaces in both core and outcrop, culminating with the uppermost channel complex that is 16 m (53 ft) thick. This reflects a stratigraphic increase in element preservation. The thin-bedded facies (CLf4 and CLf5) in this core record abundant soft-sediment deformation and are typical of channel margin deposits (Figure 4) (CLf6). The thin-bedded nature of the siltstone-prone deposit (CLf5) combined with the abundance of mudstone drapes and the increased intensity of bioturbation suggests that the system was waning and that only dilute turbidity currents were entering the basin. Figures 4 and 5 show that this uppermost 8 m (26 ft) of C2 in this well has been interpreted to be part of an abandonment unit deposited as the C2 system began to backstep and before the shutdown associated with the upper C mudstone, as described by Di Celma et al. (2011) and Flint et al. (2011).

Borehole Bav 2

In Bav 2, three C2 channel complexes have been interpreted (Figure 5) based on erosion surfaces and channel lag deposits (CLf2). The C2 channel complex set does not have the same depth of erosion as recorded in Bav 1a because the B–C interfan and 30 m (98 ft) of the overlying B–C mudstone are present

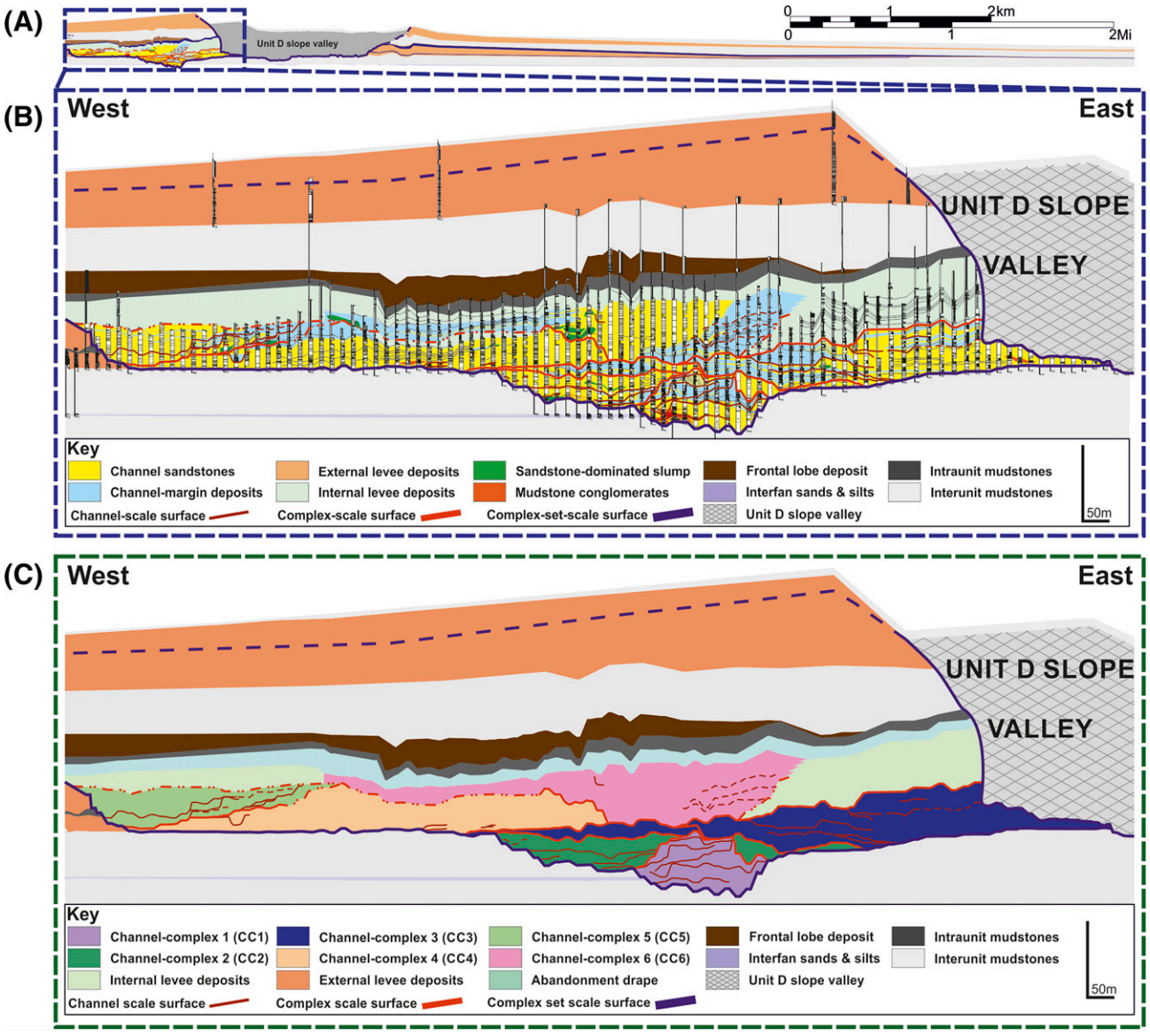

Figure 8. (A) Entire CD Ridge panel. (B) Enlarged crop of the western CD Ridge panel showing the C2 channel complex set. (C) Correlation panel showing the same enlarged crop of the CD Ridge panel showing the six main channel complexes (CC1–CC6) that are observed and correlated across the syncline.

(Figure 5). This core contains similar facies to Bav 1a, characteristic of channel axis and channel off-axis environments of deposition (Campion et al., 2000; McHargue et al., 2011), but thick channel lag deposits are absent, and there is no variation in the composition of the mudstone clasts throughout the channelized succession. Overlying the three subunit C2 channel complexes, the Bav 2 core records 27 m (90 ft) of both proximal and distal internal levee deposits (CLf3, CLf4, and CLf5) that is capped by an 8-m-thick (26-ft-thick) abandonment unit (CLf4 and CLf5).

Figure 6 is a correlation of C2 between Bav 1a and Bav 2. The correlation datum is the upper C mudstone. This panel highlights the channel elements, channel complexes, and channel complex set interpreted in each of the wells and shows that there is no clear correlation at channel element or channel complex scale over the 0.7 km (0.4 mi) interwell spacing. However, it is likely that the heterogeneous thin-bedded deposits recorded in Bav 2 acted to confine the late stage vertically stacked channel complex in Bav 1a (CC6) within the late stage erosion surface, suggesting these deposits were constructed

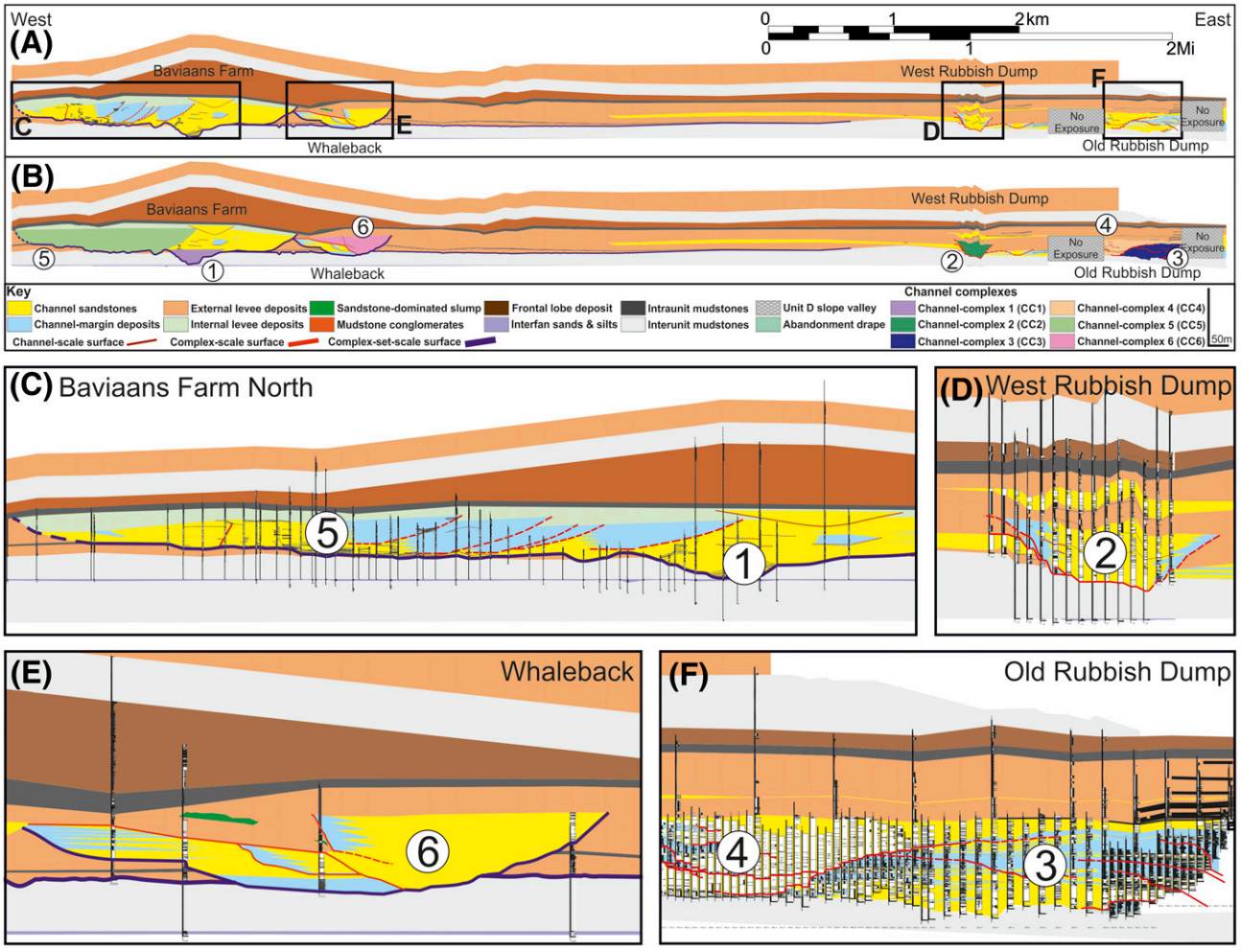

Figure 9. Correlation panels from the north limb of the Baviaans syncline: (A) Correlation panel showing units C and D, with boxes that correspond to the four enlarged panel crops in (C)–(F). (B) Units C and D with the six C2 channel complexes that correlate to the corresponding numbered channel complexes identified on the CD Ridge panel (Figure 8). (C) Enlarged panel showing CC1 and CC5 identified at Baviaans Farm. (D) Panel crop for CC2 at the West Rubbish Dump. (E) Detail panel showing CC6 at the Whaleback. (F) Enlarged panel showing CC3 and CC4 at the Old Rubbish Dump.

by this channel complex as internal levees (Kane and Hodgson, 2011).

Although it is not possible to correlate channel elements between the two wells (Figure 6), the erosion surface separating CC3 and the overlying internal levee in Bav 2 is correlated to the erosion surface at the base of CC6 in Bav 1a. Also, although CC3 is intersected in both wells, the channel remnants preserved in Bav 1a are older than those captured in Bav 2 based on stacking pattern.

Contribution of Borehole Images and Wireline Logs

The generally high gamma-ray readings in the Fort Brown Formation are caused by a high percentage of potassium feldspar in the rocks. Cross-plotting gamma-ray and sonic log values shows that among the types of thin beds, it may be possible to distinguish external levees from internal levees (Figure 7) because the external levees are a little sandier and cleaner. This plot shows that it is not possible to distinguish channel margin thin beds from either external or internal levees on conventional logs, which becomes a problem when making interpretations of architectural elements in uncored wells. The gamma-ray log for the lower half of the C2 interval in Bav 1a (Figure 4) has a spiky character with no clear internal trends. We know from outcrop control that this section of the borehole passes through CC1 and CC3 (Figure 8). The CC1 comprises stacked

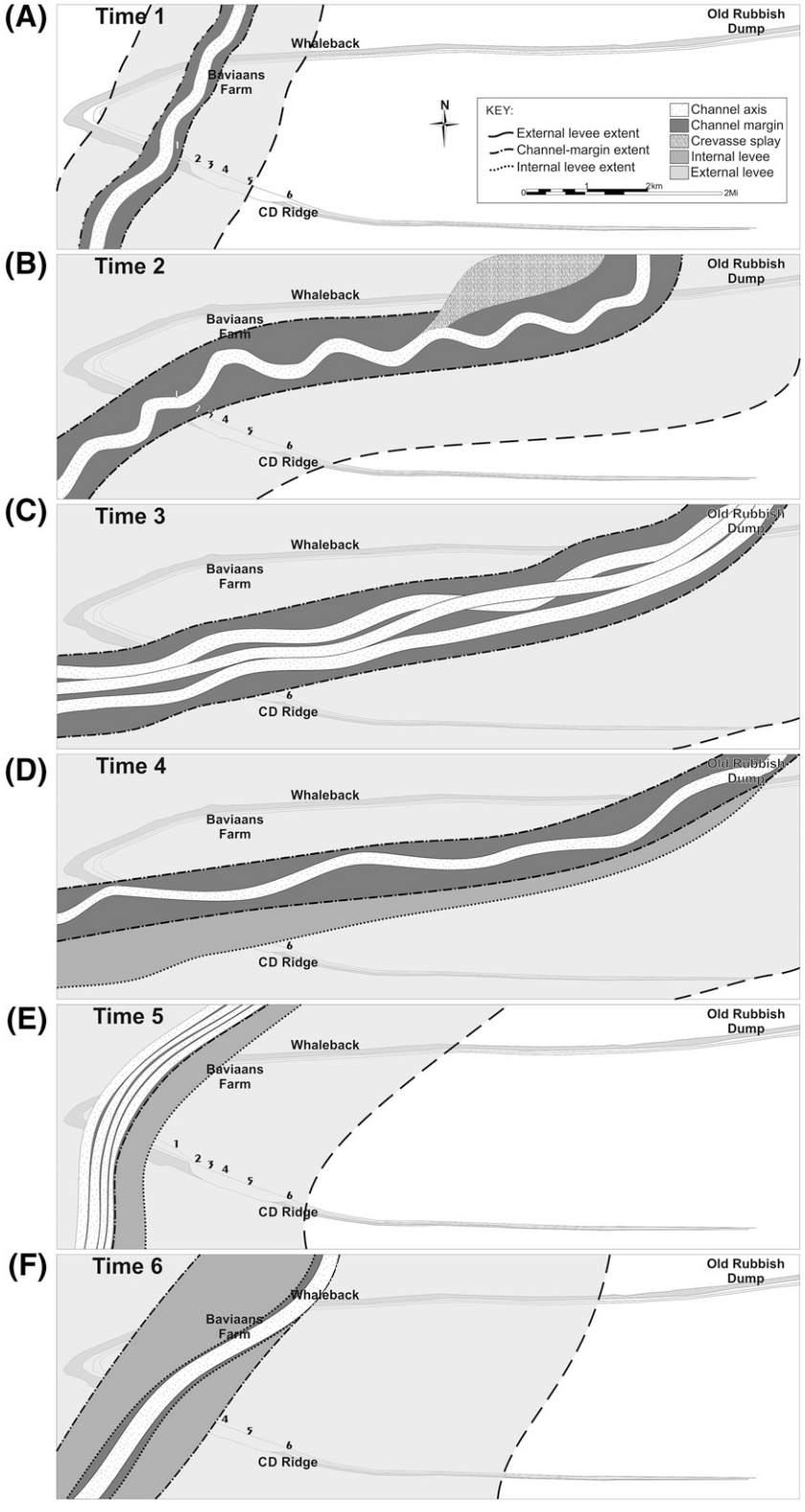

Figure 10. Paleogeographic maps, reconstructed using correlations between channel complexes identified on the north and south limbs of the Baviaans syncline. (A) The oldest channel complex (channel complex 1) observed in the study area, (B) channel complex 2, (C) channel complex 3, (D) channel complex 4, (E) channel complex 5, and (F) the youngest channel complex (channel complex 6).

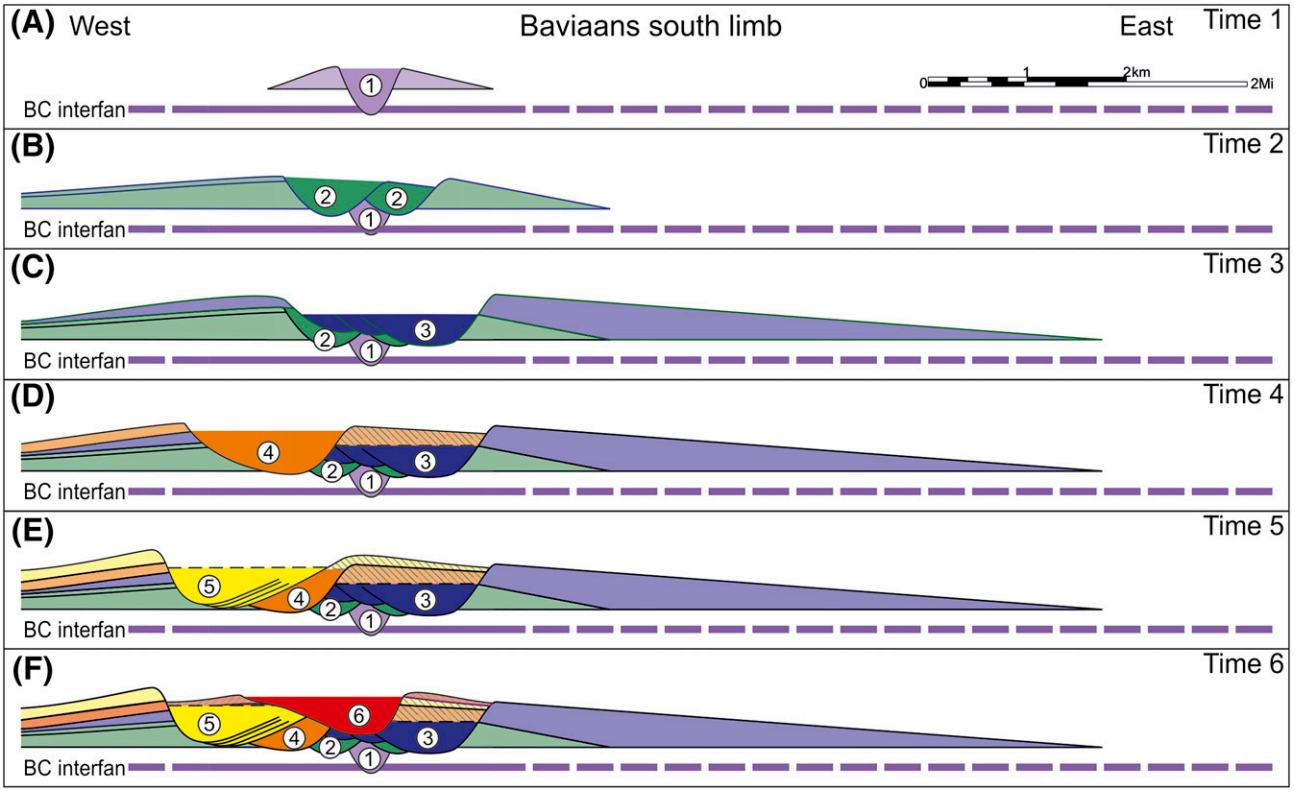

Figure 11. Cross sections combining outcrop observations from the CD ridge panel, Baviaans south limb (Figure 8) and the paleogeography maps of Figure 10, using the B–C interfan as a datum: (A) time slice 1, (B) time slice 2, (C) time slice 3, (D) time slice 4, (E) time slice 5, and (F) time slice 6.

erosional remnants of channels, the bases of each one being mantled by mudstone rip-up clasts. Three intervals of channel margin thin beds also exist, but these are only imaged clearly for one interval at 120 m (394 ft) (Figure 4). The high gamma-ray expression of this channel margin facies could easily be interpreted as a laterally extensive abandonment drape. The upper section of the borehole passes through the almost completely preserved CC6 channel complex, which shows an upward cleaning trend.

Borehole electrical images from the FMS tool were analyzed for paleocurrent information such as climbing ripples and cross-beds but also on secondary structures such as erosion surfaces and sedimentary faults (see Tables A–F, supplementary material available as AAPG Datashare 75 at www.aapg.org/datashare). The scatter of these data within the C2 channel complexes is quite large, most probably caused by channel sinuosity, channel margin collapse, and lateral stepping. In the absence of core, the borehole images are crucial in the correct identification of channel and channel complex boundaries, which can be recognized by concentrations of mudstone rip up clasts and subtle erosion surfaces that are onlapped by channel margin thin beds that display a shallowing upwards of bed dips. These features are not resolvable reliably on conventional wireline logs. Paleocurrent indicators from the unconfined deposits, particularly in the external levees, show a more coherent paleoflow pattern with a much smaller scatter in directions that are consistent with the outcrop-derived paleoflow directions (Kane and Hodgson, 2011). This paleocurrent information, together with the basal surfaces that can be identified on borehole images, is a valuable contributor to constraining reservoir models in channel–levee systems.

TWO-DIMENSIONAL OUTCROP CORRELATIONS

On the CD Ridge outcrop, six C2 channel complexes (CC1–CC6) comprising structureless channel axis

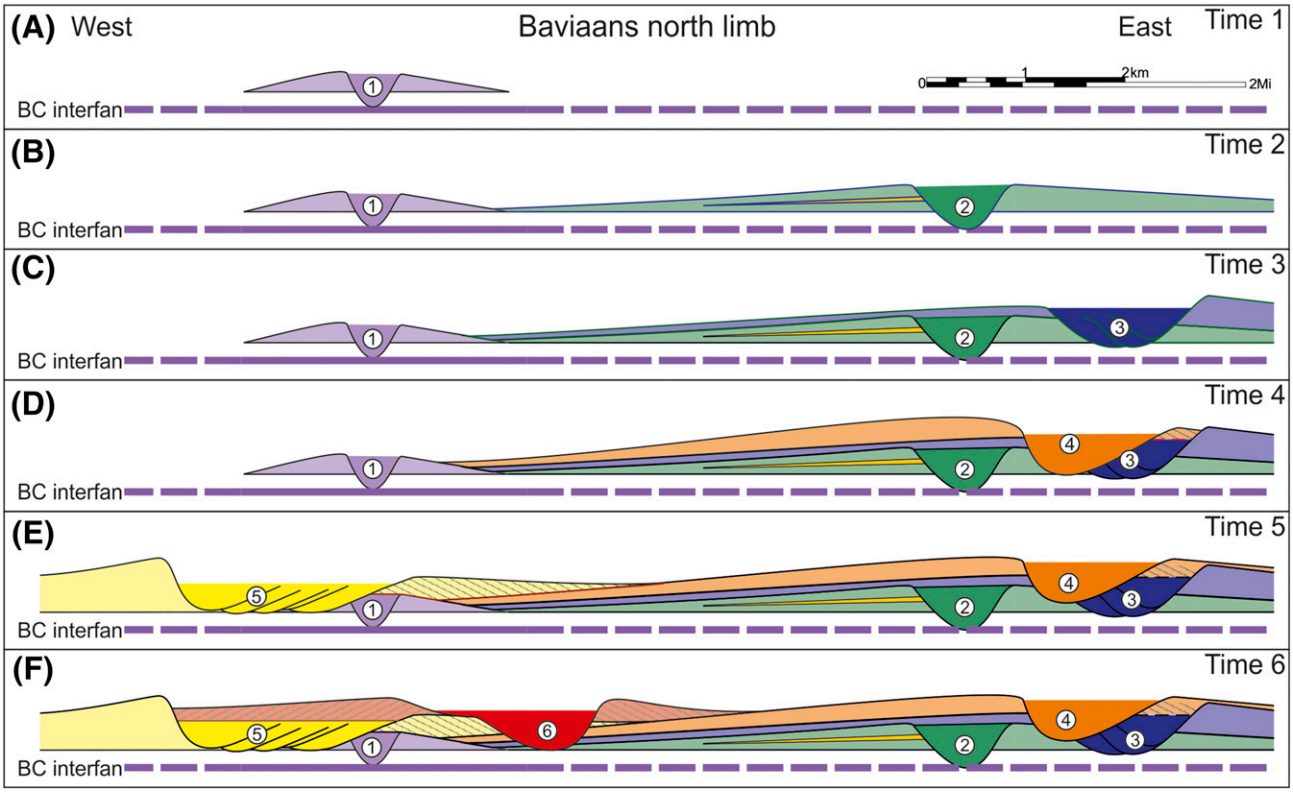

Figure 12. Cross sections combining outcrop observations from the north limb of the Baviaans syncline (Figure 9) and the paleogeography maps of Figure 10A–F, using the B–C interfan as a datum: (A) reconstructed cross section for time slice 1, (B) time slice 2, (C) time slice 3, (D) time slice 4, (E) time slice 5, and (F) time slice 6.

sandstone (CLf1 and CLf2) and thin-bedded channel margin facies (CLf4, CLf5, and CLf6) have been identified by mapping erosion surfaces where they cut into older deposits (Figure 8). The surfaces are mantled by mudstone and siltstone clasts and are onlapped by channel margin thin beds. The relative ages of the channel complexes is constrained by cross-cutting relationships (Figure 8). On the north limb of the Baviaans syncline, six corresponding channel complexes have been correlated using geometry, stacking patterns of component channels, paleocurrent data, and depths of erosion surfaces. Figure 9 shows where the numbered channel complexes crop out, their geometries, and their interpreted stratigraphic relationship.

PALEOGEOGRAPHIC RECONSTRUCTIONS

Using the combined outcrop and core observations from both limbs of the syncline, a series of paleogeographic maps (Figure 10) and cross sections (Figures 11, 12) have been constructed, detailing the evolution of the C2 channel complex set through time. Regional depositional dip for C2 is to the northeast, but individual channel complexes vary in orientation, from north to east.

Time Slice 1: Channel Complex 1

Time slice 1 (Figure 10A) correlates the oldest and deepest preserved remnant channel complex of C2 age recorded on the CD Ridge (CC1; Figure 8) to the deepest and oldest channel complex 2-km (1-mi) downdip on the north limb of the Baviaans syncline (CC1 in Figure 9). The low degree of asymmetry of the remnant complex preserved on both limbs of the syncline suggests that this channel complex had a low degree of sinuosity. The 30+ m (98+ ft) of incision on this channel complex suggests that it was mostly erosionally confined.

The cross sections for time slice 1 (Figures 11A, 12A) show the CC1 erosion surface down-cutting

into the B–C interfan on the south limb with inferred small, symmetrical external levees adjacent to it (Figure 11A). The complex shows similar features on the north limb but with basal erosion down to just above the B–C interfan (Figure 12A).

Time Slice 2: Channel Complex 2

Channel complex 2 (Figure 10B) is preserved as two remnant channel complexes on the CD Ridge, directly overlying the CC1 complex (Figure 8). These remnants are correlated to the symmetrical channel complex that incises below the base of unit C mapped out 8.5 km (5 mi) to the east–northeast near the West Dump on the north limb of the syncline (CC2; Figure 9). The asymmetry of the channel complex, with its eastward stepping constituent channel elements on the CD Ridge and the preservation of several channel margins preferentially on the western side of the complex farther downdip, implies moderate sinuosity.

The cross section for time slice 2 (Figure 11B) on the south limb shows two remnant channel complexes, both of which incise to the base of unit C, and the western complex is the youngest. We interpret asymmetric levees adjacent to these channel complexes, with the larger external levee to the west. The two channel complexes identified on the south limb are undifferentiated on the north limb, where thick external levees are inferred to have confined the CC2 complex, possibly aggrading with it. A crevasse splay deposit is present in the western external levee, captured on the outcrop correlation panel (Figure 9); its stratigraphic position in the middle of the external levee succession suggests that the channel complex and the external levees aggraded quasi-synchronously.

Time Slice 3: Channel Complex 3

Time slice 3 (Figure 10C) shows a C2-aged channel complex adjacent to the unit D slope valley on the CD Ridge (CC3; Figures 4, 5, 8). Constituent remnant channel elements show an eastward stepping stacking pattern, with channel margin material preferentially preserved to the west. This channel complex has been correlated to a channel complex at the Old Rubbish Dump (Pringle et al., 2010) exposed 10 km (6 mi) downdip (CC3; Figure 9), where channel elements record a similar eastward stepping with extensive channel margin material also preserved toward the west. Both channel complexes cut down to the stratigraphic level of base subunit C1. The asymmetry and internal eastward stepping of channel elements within the CC3 channel complexes suggest that external levee deposits associated with these channel complexes were asymmetric, with a thicker levee to the east.

The cross-section reconstruction for time slice 3 on the CD Ridge shows how a channel complex partly truncates the older, eastern CC2 channel complex, incising to the base of unit C. Individual channel elements in the CC3 channel complex are eastward stepping. On the north limb (downdip), this same deeply incised and eastward stepping channel element trend is present. We interpret that asymmetric external levees bounded the channel complex, with the higher levee on the eastern margin with preferential flow stripping and overspilling to the east as a consequence of the eastward stepping of the individual channel elements.

Time Slice 4: Channel Complex 4

Time slice 4 (Figure 10D) comprises the large, western CC4 channel complex on the CD Ridge (Figure 8). This complex incises into the westernmost exposed deposits of the CC3 channel complex, removing the stratigraphic relationship with external levee deposits. The lack of exposed channel margin deposits and channel element–scale surfaces means that the geometry of this channel complex is poorly constrained. It has been correlated to the youngest, asymmetric channel complex cropping out at the Old Rubbish Dump (Pringle et al., 2010) (CC4; Figure 9) on the north limb. The asymmetry of constituent channel elements here suggests that the channel complex was weakly sinuous in planform.

Topography on the CC3 eastern external levee on the south limb of the syncline is likely to have acted to partially confine the eastern external levee of the CC4 channel complex, forming a confined external levee. The western external levee of CC4 was not confined. This pattern is extended downdip, with the eastern CC4 external levee inferred to have been confined by topography created by the eastern external levee of CC3, whereas the CC4 western external levee

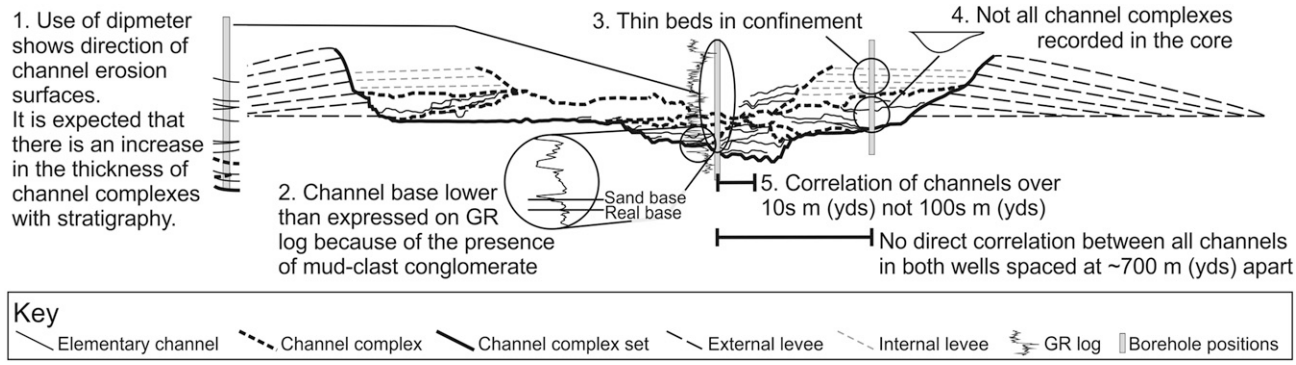

Figure 13. Key learnings from this integrated study that can be applied to exhumed and subsurface submarine channel–levee systems. GR = gamma ray.

is largely unconfined. In both correlation panels, CC4 incised through part of CC3, cutting down to the base of unit C, removing older external levee deposits genetically related to older channel complexes.

The asymmetry of the channel complex on the north limb suggests that the external levees adjacent to that channel complex are likely to have been asymmetric, with a thicker western levee at an interpreted outer bend position. The reconstructed cross section for the north limb suggests that the eastern external levee of CC3 was high enough to act as a confining surface.

Time Slice 5: Channel Complex 5

Channel complex 5 shows the paleogeographic interpretation of the westernmost C2-aged channel complexes recorded on the CD Ridge and on the north limb of the syncline opposite Baviaans Farm (Figure 10E). In both areas, the constituent channel elements show a west-stepping stacking pattern, with extensive preserved channel margin deposits (CC5; Figures 8, 9). The map shows this channel complex as sinuous with an outer bend to the west.

It is suggested that the thick eastern external levee constructed during time slice 3 on the south limb of the syncline confined the eastern external levee associated with CC5. On the north limb, the deposits of the western external levee were unconfined, and the eastern levee onlapped the western external levee of CC4, forming a composite levee succession.

Time Slice 6: Channel Complex 6

Channel complex 6 is the youngest channel complex recorded in C2 on the CD Ridge (CC6; Figures 4, 5, 8) and in Bav 1a (Figure 10F) and the most completely preserved. At outcrop, this complex is characterized by vertically stacked aggradational channel elements confined by internal levee deposits. Channel complex 6 is correlated to the complex exposed at the Whaleback, 5 km (3 mi) downdip on the north limb of the syncline (CC6; Figure 9). The channel complex at the Whaleback is asymmetric, indicating sinuosity. Internal levees overlying a CC6 erosion surface confine the late stage aggradational channel complex on both limbs of the syncline.

The northern correlation panel shows CC6 to be a highly erosive channel complex that incised through external levee deposits, constructed during time slices 2–5. It is interpreted to have been confined by external levees to the east that onlap onto older external levees constructed during time slice 4 and by an internal levee to the west.

DISCUSSION

Subsurface Implications of the One-Dimensional and Two-Dimensional Data

The integration of core and well log data to adjacent outcrops provides a link between 1-D and 2-D data and scales the well data up to field mapping scale. The correlation across the Baviaans syncline provides between 2 km (1 mi) and 10 km (6 mi) of downdip control. Figure 13 highlights five of the key learnings from this high-resolution integrated study of submarine channel complex evolution:

1. A stratigraphic trend of channel complexes and channel elements being thicker through the

channel complex set (Figure 4A) exists such that the youngest, vertically aggradational channel complex (CC6) is the best preserved in both updip and downdip data sets. On average, channel remnants are 3 m (10.5 ft) thick, channel complex remnants are 11 m (36 ft) thick, and the C2 channel complex set is 40 m (131 ft) thick. This is interpreted to reflect the increased preservation potential of younger components of a channel complex set as the deep-water system evolved from bypass-dominated to aggradational within the lowstand systems tract (Hodgson et al., 2011).

2. Although the basal surface of the C2 channel system is the most correlative, it can be difficult to pick out using well logs alone because mudstone clast conglomerate produces high gamma-ray readings. The same issue holds when trying to identify correlative channel surfaces (channel element and channel complex boundaries) in well logs. However, borehole images can be more helpful because they show basal mudstone clasts as dark (conductive) features and basal surfaces as abrupt changes in conductivity (Table 2).
3. Preservation of thin-bedded turbidites within the main composite bounding surfaces are either channel margin (Bav 1a) or internal levee deposits (Bav 2; Figures 8, 13). Therefore, it is important to consider the environment of deposition of thin beds and their connectivity to sand-rich deposits. Channel margin thin beds show similar electrofacies to external or internal levee thin beds in conventional wireline logs (Figure 7), but image logs help to distinguish between these thin bed types.
4. A single vertical well will not intersect all channel complexes. This is a combined function of lateral channel switching, stacking pattern, and sinuosity. Furthermore, a bypass surface in updip locations can be represented by multiple channel complexes downdip (Stevenson et al., 2015).
5. Boreholes Bav 1a (Figure 4) and Bav 2 (Figure 5) are 0.7 km (0.44 mi) apart, and although several channel element–scale surfaces and channel complex–scale surfaces were identified in each of the cores, none of these surfaces could be correlated with confidence between the wells (Figure 6). Typically, the correlation lengths of channel elements are less than the well spacing. However, using additional information provided in the outcrop correlation panel from the CD Ridge (Figure 8), the CC3 and CC6 erosion surfaces were correlated. Combining observations from both wells, only CC1, CC3, and CC6 were intersected in both Bav 1a and Bav 2. The hierarchy and scale of channel erosion surfaces, combined with stratigraphic position, are key when correlating and interpolating in three dimensions. Dip measurements from electrical borehole image logs can be employed to calculate the angle and direction of erosion surfaces to help with correlating these surfaces between wells.

Controls on Location and Stacking Patterns of Channels

A long-term entry point in the southwestern corner of the Baviaans syncline is interpreted as due to the presence of channelized axes of units B, C, and D (Di Celma et al., 2011; Hodgson et al., 2011; Brunt et al., 2013b; van der Merwe et al., 2014). The coeval shelf edge has been removed because of later uplift of the Cape fold belt so the mechanism for this long-term focus of supply is unknown. The paleogeographic reconstructions for C2 indicate a levee-confined channel system that bifurcates downslope into a series of isolated channel complexes. This pattern means that more of the stratigraphic history of the system is preserved as deposits on the north limb of the Baviaans syncline, with more time locked up on erosion surfaces farther updip on the CD Ridge.

The paleogeographic maps (Figure 10) show two main clusters of channel complexes on the north limb of the syncline that are separated by approximately 6 km (4 mi) of overlapping siltstone-rich external levee deposits (Figure 9). This composite external levee succession was built by overspilling and flow stripping from different channel complexes (Figure 12), although there is no evidence that more than one channel complex was active at a time. At any one time, the topography of the composite levee would influence the behavior of sediment gravity flows that escaped the active conduit. The constructional topography likely hindered the potential for an avulsion into this area.

An internal levee is defined as a constructional feature deposited lateral to a channel but within a larger confining surface (Kane and Hodgson, 2011; Hansen et al., 2015). The situation described here

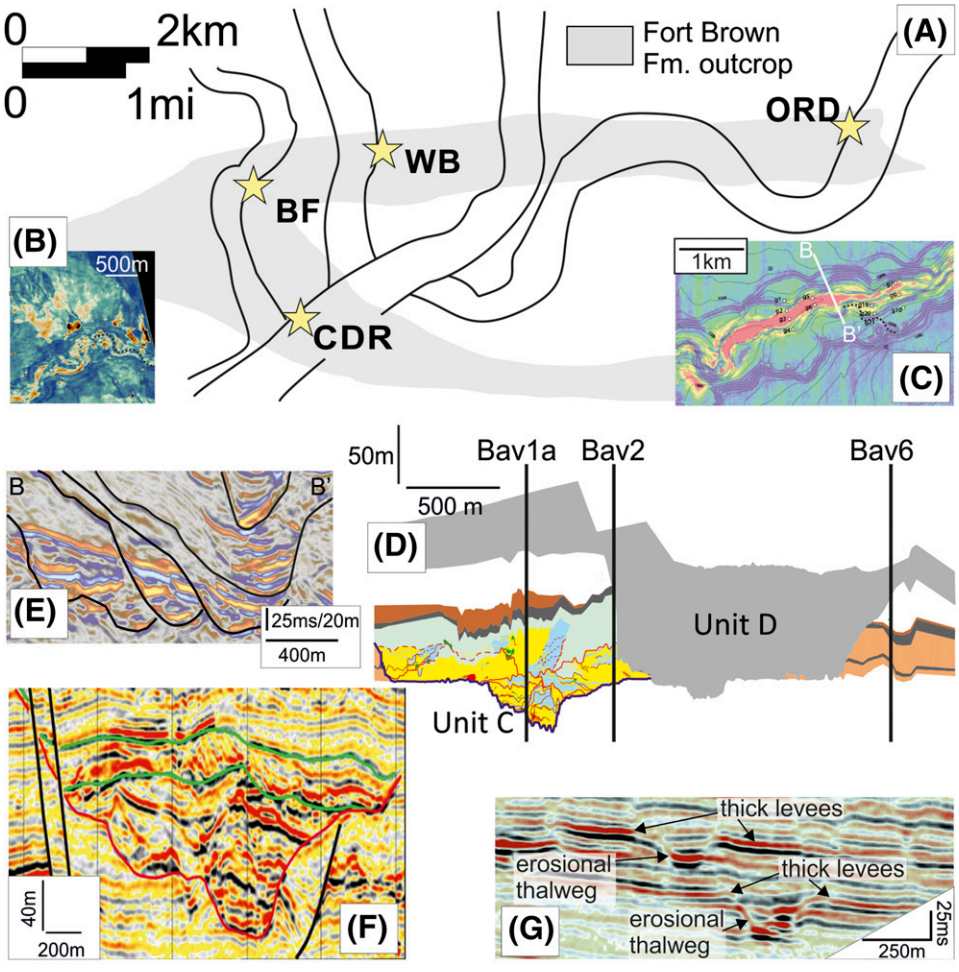

Figure 14. Planform and cross-section examples of subsurface submarine channel–levee systems scaled to the unit C system to illustrate comparable scale and architecture. The gray shape on the map is the Fort Brown Formation (Fm.), and the yellow stars refer to key localities. (A) Channel patterns from an avulsion node mapped offshore Niger delta (Armitage et al., 2012, used with permission of AAPG) that shares a similar rate of divergence. (B) Map of a Miocene hybrid channel from offshore West Africa with a combination of early incision and later construction of external levees, as interpreted from the Laingsburg C2 succession. Adapted from Janocko et al. (2013), with permission from Elsevier. (C) Map view of a seabed submarine channel system, the Y channel, from offshore Nigeria. Adapted from Jobe et al. (2015). (D) Unit C in the CD ridge, adapted from Figure 3B. (E) Seismic cross section through the Y channel, from offshore Nigeria. Note the lateral to aggradational stacking pattern at a similar scale to the complexes in unit C2. Adapted from Jobe et al. (2015). (F) Seismic profile from the Dalia M9 Upper Channel System, adapted from Abreu et al. (2003), with permission from Elsevier. Note the similar architecture. Red line is the base of the system, and the youngest channel complex is highlighted by green lines. (G) Seismic section through two hybrid channels with erosional and levee confinement, from offshore West Africa, adapted from Janocko et al. (2013), with permission from Elsevier. Note apparent simplicity of the channelized part in contrast to the C2 stratigraphy in (D). BF = Baviaans Farm; CDR = CD Ridge; ORD = Old Rubbish Dump; WB = Whaleback.

between the western and eastern channel axes is different because the external levees were partially confined by constructional topography of older external levees. The term "confined external levee" is introduced here for levees that are deposited outside the channel belt confining surface but subject to the influence of underlying constructional topography. External levees are commonly seen to onlap each other in seismic section (e.g., McHargue and Webb, 1986; Bastia et al., 2010; Catterall et al., 2010), and the area between the western and eastern channel complexes is interpreted as an outcrop example of this situation. The sedimentary processes within a confined external levee deposit and an internal levee may be similar; therefore, the sedimentary facies may share affinities, such as deflection of flows by the confining surface, recorded by multidirectional current and climbing ripple cross-lamination (Kane and Hodgson, 2011). Also, flows within a confined external levee cannot travel as far from the parent conduit as those within an unconfined external levee, which will influence bed thickness patterns and bed geometries. In the hierarchy used here, these composite external levees would represent an external levee complex set; however, it has not yet been possible to distinguish constituent external levee complexes and external levee elements.

Scale and Architectural Comparison to Other Systems

The unit C lowstand sequence set is up to 80 m (260 ft) thick in the study area; it overlies the 50-m-thick (165-ft-thick) B–C mudstone, and is overlain by the 26-m-thick (85-ft-thick) C–D mudstone. These thicknesses and likely strong acoustic impedance contrasts at base and top of unit C suggest the succession would be mappable in many deep-water seismic reflection data sets. Although the two outcrop panels provide a wealth of architectural data in two dimensions, augmented by the boreholes, the map view geometries are interpreted instead of directly imaged. In recent years, there have been many publications showing map view geometries derived from seismic amplitude horizon slices through slope channel–levee complexes and slope valleys. In most cases, the systems imaged are at the whole unit C scale. Notwithstanding this resolution difference, and mindful of the well-developed hierarchy in deep-water systems, such map view images provide a useful constraint on the geometries interpreted within C2. Figure 14 shows a horizon slice and cross section through Cenozoic slope deposits, offshore West Africa (Abreu et al., 2003; Armitage et al., 2012; Janocko et al., 2013; Jobe et al., 2015). The horizontal distance scales well with the distance across the Baviaans syncline, and the 25-ms (~25-m [82-ft]) vertical scale suggests that the channel features are only a little larger than the C2 channel complexes. What is mappable as a channel element is likely a channel complex in outcrop and well data (Figures 13, 14).

To obtain map view images of features that scale with outcrop-scale vertical resolution requires either extremely high–resolution shallow seismic data or studies of the modern seabed. A comprehensively studied Pleistocene slope channel example is the Lucia Chica system, offshore central California. High-resolution data collected by autonomous underwater vehicle radar surveys provide information at similar resolution to the C2 channel complexes (Maier et al., 2011, 2012, 2013). The system was active during the last glacioeustatic lowstand and was abandoned at 11 ka during the postglacial sea-level rise. Maier et al. (2013) documented the evolution of four channels, which initiated as erosional features and subsequently developed levees, in a similar mechanism envisioned herein.

Janocko et al. (2013) described hybrid channels that show characteristics of both erosional and levee-confined types, which we interpret to be the dominant style in C2. The high-resolution data from Lucia Chica led Maier et al. (2013) to argue that the channels in that system evolved from erosional to levee confined, before avulsion occurred. Older channels have thicker levees, higher sinuosity, and evidence of lateral stepping. A similarity between the Lucia Chica system (Maier et al., 2012), the Y channel (Jobe et al., 2015), and C2 is that lateral movement of channels was achieved through lateral stepping instead of lateral migration.

An Exhumed Example of an Avulsion Node

The CD Ridge area marks a site that was prone to multiple abrupt changes in the pathways of channel complexes and is interpreted as a unique example of an exhumed deep-water avulsion node. Three types of avulsion pattern have been noted in deep-water channel systems. These include forward-stepping, back-stepping, radial, and single node (Kolla, 2007; Armitage et al., 2012; Pyles et al., 2014). Triggers for avulsion events include allocyclic controls such as changes in climate, sea level, or tectonics (Kolla, 2007; Maier et al., 2012). Autocyclic controls may include increasing channel sinuosity (Kolla, 2007), limited downstream accommodation, and backfilling of individual channel thalwegs caused by lobe deposition (Prélat et al., 2010) or breaching of a levee and response to a changed base level (Fildani et al., 2006; Brunt et al., 2013a; Covault et al., 2014; Ortiz-Karpf et al., 2015). However, the lack of longitudinal migration of the C2 avulsion node points to an underlying control, such as a break-in-slope, although this is too subtle to resolve at outcrop. The channel complexes were not active at the same time, so the pattern is not bifurcation; however, the map view pattern and scale of channel complex divergence are remarkably similar to those identified by Armitage et al. (2012) (Figure 14). In the Lucia Chica system, Maier et al. (2013) suggested overall low channel relief, and highly asymmetrical channel levees influenced the position of an avulsion node, which is a situation common in the C2 succession.

The area downdip of the avulsion node (the north limb) in C2 is notable for the lack of sand-rich

frontal lobe deposits, although they are interpreted at the base of the underlying subunit C1 (Di Celma et al., 2011) and overlying subunit C3 (Morris et al., 2014b). The wide belt of channel complexes and composite external levees on the north side of the Baviaans syncline suggests that the absence of frontal lobes at the base of C2 external levees cannot be ascribed to low preservation potential and indicates persistent sediment bypass of high-energy flows (Stevenson et al., 2015). Sand-rich C2 lobe deposits are found approximately 25 km (15.5 mi) downdip of the study area (Di Celma et al., 2011; Brunt et al., 2013a), which is consistent with an accommodation-limited slope in the study area, such that flows remained in sand bypass mode. Deposition of a crevasse or frontal lobe (or splay) is common where there is available accommodation following an initial breach of an external levee (Fildani et al., 2006). Depending on usable accommodation, flows will deposit rapidly (e.g., Parsons et al., 2002; Hall and Ewing, 2007; Morris et al., 2014b). As the system stabilizes, a channel and levee may develop over the lobe (Lopez, 2001; Maier et al., 2012). High-amplitude continuous-to-discontinuous reflection packages (Posamentier and Kolla, 2003) are preserved between or underlying channel and levee deposits, as identified in the Amazon, Indus, Zaire, and Bengal fan systems (Damuth et al., 1988; Flood et al., 1991; Normark et al., 1997; Pirmez et al., 1997, 2000; Lopez, 2001; Droz et al., 2003; Kolla, 2007). However, Ortiz-Karpf et al. (2015) provide a subsurface example of a deep-water avulsion cycle where there is a zone between the point of avulsion and the updip pinchout of the avulsion lobe. The implication is that not all avulsion nodes will be associated spatially with sand-rich frontal lobe deposits, which is an important consideration in subsurface reservoir prediction.

CONCLUSIONS

The C2 deep-water slope system shows a temporal evolutionary trend in the style of constituent channel complexes and in the nature of external levees. The oldest and most deeply incised channel complex is overlain by a series of external levee-confined, laterally stepping asymmetric channel complexes succeeded by an aggradational channel complex confined by internal and external levees. The older complexes are only partly preserved because of deep erosion on complex boundaries. Constituent channels are similarly preserved remnants, with no consistent aspect ratios. Channel and channel complex boundaries are marked by combinations of mudstone clast accumulations and channel margin or internal levee thin beds that onlap erosion surfaces. Neither of these expressions can be reliably picked on conventional wireline logs and, in the absence of core, image logs are vital for accurate interpretations.

Moving 2–5 km (1–3 mi) downdip, the external levees overlap to form a thick composite external levee succession that was supplied by flows escaping from channel complexes of different ages and spatial positions. The external levees genetically related to the younger channel complexes were partially confined because of topography created through deposition of unconfined external levees associated with the older channel complexes 1–3. The facies in these confined external levees are similar to those of internal levees. The growth of this confined external levee complex inhibited channel avulsion, resulting in two preferential pathways being used by channel complexes.

The downdip change over 2–5 km (1–3 mi) from a narrow, focused system to a more dispersed system is interpreted to record an exhumed deep water avulsion node. The position of the node may reflect a structural control such as a break in slope. Frontal lobes, crevasse lobes, or splays are commonly associated with avulsion nodes; however, these features are not present in the Baviaans study area, and instead they have been observed approximately 25 km (15.5 mi) downdip. This suggests that the channels remained in sand bypass mode.

REFERENCES CITED

Abreu, V., M. Sullivan, C. Pirmez, and D. Mohrig, 2003, Lateral accretion packages (LAPs): An important reservoir element in deep water sinuous channels: Marine and Petroleum Geology, v. 20, p. 631–648, doi:10.1016/j.marpetgeo.2003.08.003.

Armitage, D. A., T. McHargue, A. Fildani, and S. A. Graham, 2012, Post-avulsion channel evolution: Niger Delta continental slope: AAPG Bulletin, v. 96, no. 5, p. 823–843, doi:10.1306/09131110189.

Babonneau, N., B. Savoye, M. Cremer, and M. Bez, 2004, Multiple terraces within the deep incised Zaire Valley (Zaïango Project): are they confined levees? *in* S. A. Lomas

and P. Joseph, eds., Confined turbidite systems: Geological Society, London, Special Publications 2004, v. 222, p. 91–114, doi:10.1144/GSL.SP.2004.222.01.06.

Babonneau, N., B. Savoye, M. Cremer, and B. Klein, 2002, Morphology and architecture of the present canyon and channel system of the Zaire deep-sea fan: Marine and Petroleum Geology, v. 19, p. 445–467, doi:10.1016/S0264-8172(02)00009-0.

Badalini, G., B. Kneller, and C. D. Winker, 2000, Architecture and processes in the Late Pleistocene Brazos-Trinity turbidite system, Gulf of Mexico continental slope, *in* P. Weimer, R. M. Slatt, J. Coleman, N. C. Rosen, H. Nelson, A. H. Bouma, M. J. Styzen, and D. T. Lawrence, eds., Global deep-water reservoirs: Gulf Coast Section SEPM Foundation 20th Annual Bob F. Perkins Research Conference, Houston, Texas, December 3–6, 2000, p. 16–34, doi:10.5724/gcs.00.15.0016.

Badescu, M. O., C. A. Visser, and M. E. Donselaar, 2000, Architecture of Thick-bedded deep-marine sandstones of the Vocontian Basin, SE France, *in* P. Weimer, R. M. Slatt, J. Coleman, N. C. Rosen, H. Nelson, A. H. Bouma, M. J. Styzen, and D. T. Lawrence, eds., Global deep-water reservoirs: Gulf Coast Section SEPM Foundation 20th Annual Bob F. Perkins Research Conference, Houston, Texas, December 3–6, 2000, p. 35–39, doi:10.5724/gcs.00.15.0035.

Bastia, R., S. Das, and M. Radhakrishna, 2010, Pre- and post-collisional depositional history in the upper and middle Bengal fan and evaluation of deepwater reservoir potential along the northeast Continental Margin of India: Marine and Petroleum Geology, v. 27, p. 2051–2061, doi:10.1016/j.marpetgeo.2010.04.007.

Beaubouef, R. T., 2004, Deep-water leveed-channel complexes of the Cerro Toro Formation, Upper Cretaceous, southern Chile: AAPG Bulletin, v. 88, no. 11, p. 1471–1500, doi:10.1306/06210403130.

Beaubouef, R. T., C. Rossen, F. B. Zelt, M. D. Sullivan, D. C. Mohrig, and D. C. Jennette, 1999, Deep-water sandstones, Brushy Canyon Formation, west Texas: Field guide, Hedberg Field Research Conference, April 15-20, 1999: AAPG Continuing Education Course Note Series 40, 48 p.

Blikeng, B., and E. Fugelli, 2000, Application of results from outcrops of the deep-water Brushy Canyon Formation, Delaware Basin, as analogues from the deep-water exploration targets on the Norwegian Shelf, *in* P. Weimer, R. M. Slatt, J. Coleman, N. C. Rosen, H. Nelson, A. H. Bouma, M. J. Styzen, and D. T. Lawrence, eds., Global deep-water reservoirs: Gulf Coast Section SEPM Foundation 20th Annual Bob F. Perkins Research Conference, Houston, Texas, December 3–6, 2000, p. 806–816, doi:10.5724/gcs.00.15.0061.

Browne, G. H., and R. M. Slatt, 2002, Outcrop and behind-outcrop characterization of a late Miocene slope fan system, Mt. Messenger Formation, New Zealand: AAPG Bulletin, v. 86, no. 5, p. 841–862.

Brunt, R. L., C. N. Di Celma, D. M. Hodgson, S. S. Flint, J. P. Kavanagh, and W. C. van der Merwe, 2013a, Driving a channel through a levee when the levee is high: An outcrop example of submarine down-dip entrenchment: Marine and Petroleum Geology, v. 41, p. 134–145, doi:10.1016/j.marpetgeo.2012.02.016.

Brunt, R. L., D. M. Hodgson, S. S. Flint, J. K. Pringle, C. N. Di Celma, A. Prélat, and M. Grecula, 2013b, Confined to unconfined: Anatomy of a base of slope succession, Karoo Basin, South Africa: Marine and Petroleum Geology, v. 41, p. 206–221, doi:10.1016/j.marpetgeo.2012.02.007.

Campion, K. M., A. R. Sprague, D. Mohrig, R. W. Lovell, P. A. Drzewiecki, M. D. Sullivan, J. A. Ardill, G. N. Jensen, and D. K. Sickafoose, 2000, Outcrop expression of confined channel complexes, *in* P. Weimer, R. M. Slatt, J. Coleman, N. C. Rosen, H. Nelson, A. H. Bouma, M. J. Styzen, and D. T. Lawrence, eds., Global deep-water reservoirs: Gulf Coast Section SEPM Foundation 20th Annual Bob F. Perkins Research Conference, Houston, Texas, December 3–6, 2000, p. 127–150.

Catterall, V., J. Redfern, R. L. Gawthorpe, D. Hansen, and M. Thomas, 2010, Architectural style and quantification of a submarine channel-levee system located in a structurally complex area: Offshore Nile Delta: Journal of Sedimentary Research, v. 80, p. 991–1017, doi:10.2110/jsr.2010.084.

Catuneanu, O., P. J. Hancox, and B. S. Rubidge, 1998, Reciprocal flexural behaviour and contrasting stratigraphies: A new basin development model for the Karoo retroarc foreland system, South Africa: Basin Research, v. 10, p. 417–439, doi:10.1046/j.1365-2117.1998.00078.x.

Clark, J. D., and A. R. Gardiner, 2000, Outcrop analogues for deep-water channel and levee genetic units from the Grés d'Annot turbidite system, SE France, *in* P. Weimer, R. M. Slatt, J. Coleman, N. C. Rosen, H. Nelson, A. H. Bouma, M. J. Styzen, and D. T. Lawrence, eds., Global deep-water reservoirs: Gulf Coast Section SEPM Foundation 20th Annual Bob F. Perkins Research Conference, Houston, Texas, December 3–6, 2000, p. 175–190.

Covault, J. A., S. Kostic, C. K. Paull, H. F. Ryan, and A. Fildani, 2014, Submarine channel initiation, filling and maintenance from seafloor geomorphology and morphodynamic modelling of cyclic steps: Sedimentology, v. 61, p. 1031–1054, doi:10.1111/sed.12084.

Cross, N. E., A. Cunningham, R. J. Cook, A. Taha, E. Esmaie, and N. El Swidan, 2009, Three-dimensional seismic geomorphology of a deep-water slope-channel system: The Sequoia field, offshore west Nile Delta, Egypt: AAPG Bulletin, v. 93, no. 8, p. 1063–1086, doi:10.1306/05040908101.

Damuth, J. E., R. D. Flood, R. O. Kowsmann, R. H. Belderson, and M. A. Gorini, 1988, Anatomy and growth pattern of Amazon deep-sea fan as revealed by long-range side-scan sonar (GLORIA) and high-resolution seismic studies: AAPG Bulletin, v. 72, no. 8, p. 885–911.

Deptuck, M. E., G. S. Steffens, M. Barton, and C . Pirmez, 2003, Architecture and evolution of upper fan channel belts on the Niger Delta slope and in the Arabian Sea: Marine and Petroleum Geology, v. 20, p. 649–676, doi:10.1016/j.marpetgeo.2003.01.004.

Deptuck, M. E., Z. Sylvester, C. Pirmez, and C. O'Byrne, 2007, Migration-aggradation history and 3-D seismic

geomorphology of submarine channels in the Pleistocene Benin-major Canyon, western Niger Delta slope: Marine and Petroleum Geology, v. 24, p. 406–433, doi:10.1016/j.marpetgeo.2007.01.005.

De Wit, M., and I. G. D. Ransome, 1992, Regional inversion tectonics along the southern margin of Gondwana, *in* M. J. De Wit and I. G. D. Ransome, eds., Inversion tectonics of the Cape Fold Belt, Karoo and Cretaceous Basins of southern Africa: Rotterdam, The Netherlands, A. A. Balkema, p. 15–21.

Di Celma, C. N., R. L. Brunt, D. M. Hodgson, S. S. Flint, and J. P. Kavanagh, 2011, Spatial and temporal evolution of a Permian submarine slope channel-levee system, Karoo Basin, South Africa: Journal of Sedimentary Research, v. 81, p. 579–599, doi:10.2110/jsr.2011.49.

Droz, L., T. Marsset, H. Ondreas, M. Lopez, B. Savoye, and F. L. Spy-Anderson, 2003, Architecture of an active mud-rich turbidite system: The Zaire Fan (Congo–Angola margin southeast Atlantic): Results from ZaïAngo 1 and 2 cruises: AAPG Bulletin, v. 87, no. 7, p. 1145–1168, doi:10.1306/03070300013.

Figueiredo, J. J. P., D. M. Hodgson, S. S. Flint, and J. P. Kavanagh, 2010, Depositional environments and sequence stratigraphy of an exhumed Permian mudstone-dominated submarine slope succession, Karoo Basin, South Africa: Journal of Sedimentary Research, v. 80, p. 97–118, doi:10.2110/jsr.2010.002.

Fildani, A., N. J. Drinkwater, A. Weislogel, T. McHargue, D. M. Hodgson, and S. S. Flint, 2007, Age controls on the Tanqua and Laingsburg deep-water systems: New insights on the evolution and sedimentary fill of the Karoo Basin, South Africa: Journal of Sedimentary Research, v. 77, no. 11, p. 901–908, doi:10.2110/jsr.2007.088.

Fildani, A., W. R. Normark, S. Kostic, and G. Parker, 2006, Channel formation by flow-stripping: Large-scale scour features along the Monterey East channel and their relation to sediment waves: Sedimentology, v. 53, p. 1265–1287, doi:10.1111/j.1365-3091.2006.00812.x.

Flint, S. S., D. M. Hodgson, A. R. Sprague, R. L. Brunt, W. C. van der Merwe, J. J. P. Figueiredo, A. Prélat, D. Box, C. N. Di Celma, and J. P. Kavanagh, 2011, Depositional architecture and sequence stratigraphy of the Karoo basin floor to shelf edge succession, Laingsburg depocentre, South Africa: Marine and Petroleum Geology, v. 28, p. 658–674, doi:10.1016/j.marpetgeo.2010.06.008.

Flood, R. D., P. L. Manley, R. O. Kowsmann, C. J. Appi, and C. Pirmez, 1991, Seismic facies and Late Quaternary growth of Amazon submarine fan, *in* P. Weimer and M. H. Link, eds., Seismic facies and sedimentary processes of modern and ancient submarine: New York, Springer, p. 415–433, doi:10.1007/978-1-4684-8276-8_23.

Gardner, M. H., J. M. Borer, J. J. Melick, N. Mavilla, M. Dechesne, and R. N. Wagerle, 2003, Stratigraphic process-response model for submarine channels and related features from studies of Permian Brushy Canyon outcrops, west Texas: Marine and Petroleum Geology, v. 20, p. 757–787, doi:10.1016/j.marpetgeo.2003.07.004.

Grecula, M., S. S. Flint, H. D. Wickens, and S. D. Johnson, 2003, Upward-thickening patterns and lateral continuity of Permian sand-rich turbidite channel fills, Laingsburg Karoo, South Africa: Sedimentology, v. 50, p. 831–853, doi:10.1046/j.1365-3091.2003.00576.x.

Hall, J. W., and D. Ewing, 2007, Three-dimensional turbulent wall jets issuing from moderate aspect-ratio rectangular channels: AIAA Journal, v. 45, p. 1177–1186, doi:10.2514/1.20386.

Hansen, L. A., R. H. Callow, I. A. Kane, F. Gamberi, M. Rovere, B. T. Cronin, and B. C. Kneller, 2015, Genesis and character of thin-bedded turbidites associated with submarine channels: Marine and Petroleum Geology, v. 67, p. 852–879, doi:10.1016/j.marpetgeo.2015.06.007.

Hodgson, D. M., C. N. Di Celma, R. L. Brunt, and S. S. Flint, 2011, Submarine slope degradation and aggradation and the stratigraphic evolution of channel-levee systems: Journal of the Geological Society, v. 168, p. 625–628, doi:10.1144/0016-76492010-177.

Hodgson, D. M., S. Flint, D. Hodgetts, N. J. Drinkwater, E. P. Johannessen, and S. M. Luthi, 2006, Stratigraphic evolution of fine-grained submarine fan systems, Tanqua depocenter, Karoo Basin, South Africa: Journal of Sedimentary Research, v. 76, no. 1, p. 20–40, doi:10.2110/jsr.2006.03.

Hodgson, D. M., I. A. Kane, S. S. Flint, R. L. Brunt, and A. Ortiz Karpf, 2016, Time-transgressive confinement on the slope and the progradation of basin-floor fans: Implications for the sequence stratigraphy of deep-water deposits: Journal of Sedimentary Research, v. 86, p. 73–86, doi:10.2110/jsr.2016.3.

Hubbard, S. M., J. A. Covault, A. Fildani, and B. W. Romans, 2014, Sediment transfer and deposition in slope channels: Deciphering the record of enigmatic deep-sea processes from outcrop: Geological Society of America Bulletin, v. 126, p. 857–871, doi:10.1130/B30996.1.

Hubbard, S. M., B. W. Romans, and S. A. Graham, 2008, Deep-water foreland basin deposits of the Cerro Toro Formation, Magallanes basin, Chile: Architectural elements of a sinuous basin axial channel belt: Sedimentology, v. 55, p. 1333–1359, doi:10.1111/j.1365-3091.2007.00948.x.

Janocko, M., W. Nemec, S. Henriksen, and M. Warchol, 2013, The diversity of deep-water sinuous channel belts and slope valley-fill complexes: Marine and Petroleum Geology, v. 41, p. 7–34, doi:10.1016/j.marpetgeo.2012.06.012.

Jobe, Z. R., Z. Sylvester, A. O. Parker, N. Howes, N. Slowey, and C. Pirmez, 2015, Rapid adjustment of submarine channel architecture to changes in sediment supply: Journal of Sedimentary Research, v. 85, p. 729–753, doi:10.2110/jsr.2015.30.

Kane, I. A., and D. M. Hodgson, 2011, Sedimentological criteria to differentiate submarine channel levee subenvironments: Exhumed examples from the Rosario Fm. (Upper Cretaceous) of Baja California, Mexico, and the Fort Brown Fm. (Permian), Karoo Basin, S. Africa: Marine and Petroleum Geology, v. 28, p. 807–823, doi:10.1016/j.marpetgeo.2010.05.009.

Kolla, V., 2007, A review of sinuous channel avulsion patterns in some major deep-sea fans and factors controlling them: Marine and Petroleum Geology, v. 24, p. 450–469, doi:10.1016/j.marpetgeo.2007.01.004.

Lopez, M., 2001, Architecture and depositional pattern of the Quaternary deep-sea fan of the Amazon: Marine and Petroleum Geology, v. 18, p. 479–486, doi:10.1016/S0264-8172(00)00071-4.

Luthi, S. M., D. M. Hodgson, C. R. Geel, S. Flint, J. W. Goedbloed, N. J . Drinkwater, and E. P . Johannessen, 2006, Contribution of research borehole data to modelling fine-grained turbidite reservoir analogues, Permian Tanqua-Karoo basin floor fans (South Africa): Petroleum Geoscience, v. 12, p. 175–190, doi:10.1144/1354-079305-693.

Macauley, R. V., and S. M. Hubbard, 2013, Slope channel sedimentary processes and stratigraphic stacking, Cretaceous Tres Pasos Formation, slope system, Chilean Patagonia: Marine and Petroleum Geology, v. 41, p. 146–162, doi:10.1016/j.marpetgeo.2012.02.004.

Maier, K. L., A. Fildani, T. R. McHargue, C. K. Paull, S. A. Graham, and D. W. Caress, 2013, Deep-sea channel evolution and stratigraphic architecture from inception to abandonment from high-resolution Autonomous Underwater Vehicle surveys offshore central California: Sedimentology, v. 60, p. 935–960, doi:10.1111/j.1365-3091.2012.01371.x.

Maier, K. L., A. Fildani, C. K. Paull, S. A. Graham, T. R. McHargue, and D. W. Caress, 2011, The elusive character of discontinuous deep-water channels: New insights from Lucia Chica channel system, offshore California: Geology, v. 39, p. 327–330, doi:10.1130/G31589.1.

Maier, K. L., A. Fildani, C. K. Paull, T. R. McHargue, S. A. Graham, and D. W. Caress, 2012, Punctuated deep-water channel migration: High-resolution subsurface data from the Lucia Chica channel system, offshore California, U.S.A.: Journal of Sedimentary Research, v. 82, p. 1–8, doi:10.2110/jsr.2012.10.

Masalimova, L. U., D. R. Lowe, G. R. Sharman, P. R. King, and M. J. Arnot, 2016, Outcrop characterization of a submarine channel-lobe complex: The Lower Mount Messenger Formation, Taranaki Basin, New Zealand: Marine and Petroleum Geology, v. 71, p. 360–390, doi:10.1016/j.marpetgeo.2016.01.004.

Mayall, M. J., E. Jones, and M. Casey, 2006, Turbidite channel reservoirs—Key elements in facies prediction and effective development: Marine and Petroleum Geology, v. 23, p. 821–841, doi:10.1016/j.marpetgeo.2006.08.001.

McHargue, T., M. J. Pyrcz, M. D. Sullivan, J. D. Clark, A. Fildani, B. W. Romans, J. A. Covault, M. Levy, H. W. Posamentier, and N. J. Drinkwater, 2011, Architecture of turbidite channel systems on the continental slope: Patterns and predictions: Marine and Petroleum Geology, v. 28, p. 728–743, doi:10.1016/j.marpetgeo.2010.07.008.

McHargue, T. R., and J. E. Webb, 1986, Internal geometry, seismic facies, and petroleum potential of canyons and inner fan channels of the Indus submarine fan: AAPG Bulletin, v. 70, no. 2, p. 161–180.

Menard, H. W., 1955, Deep-sea channels, topography and sedimentation: AAPG Bulletin, v. 39, no. 2, p. 236–255.

Morris, E. A., D. M. Hodgson, R. L. Brunt, and S. Flint, 2014a, Origin, evolution and anatomy of silt-prone submarine external levées: Sedimentology, v. 61, p. 1734–1763, doi:10.1111/sed.12114.

Morris, E. A., D. M. Hodgson, S. Flint, R. L. Brunt, P. Butterworth, and J. Verhaeghe, 2014b, Sedimentology, stratigraphic architecture and depositional context of submarine frontal lobe complexes: Journal of Sedimentary Research, v. 84, p. 763–780, doi:10.2110/jsr.2014.61.

Normark, W. R., 1970, Growth patterns of deep-sea fans: AAPG Bulletin, v. 54, no. 11, p. 2170–2195.

Normark, W. R., and P. R. Carson, 2003, Giant submarine canyons: Is size any clue to their importance in the rock record?: Geological Society of America. Special Paper, v. 370, p. 175–190.

Normark, W. R., and J. E. Damuth, and the Leg 155 Sedimentology Group, 1997, Sedimentary facies and associated depositional elements of the Amazon Fan, *in* R. D. Flood, D. J. W. Piper, A. Klaus, and L. C. Peterson, eds., Proceedings of the Ocean Drilling Project, Scientific Results 155, College Station, Texas, Ocean Drilling Program, p. 611–651, doi:10.2973/odp.proc.sr.155.247.1997.

Normark, W. R., D. J. W. Piper, B. R. Romans, J. A. Covault, P. Dartnell, and R. W. Sliter, 2009, Submarine canyon and fan systems of the California continental borderland, *in* H. J. Lee and W. R. Normark, eds., Earth science in the urban ocean: The southern California continental borderland: Geological Society of America Special Paper 454, p. 141–168, doi:10.1130/2009.2454(2.7).

Ortiz-Karpf, A., D. M. Hodgson, and W. D. McCaffrey, 2015, The role of mass-transport complexes in controlling channel avulsion and the subsequent sediment dispersal patterns on an active margin: The Magdalena Fan, offshore Colombia: Marine and Petroleum Geology, v. 64, p. 58–75, doi:10.1016/j.marpetgeo.2015.01.005.

Parsons, J. D., W. J. Schweller, C. W. Stelting, J. B. Southard, W. J. Lyons, and J. P . Grotzinger, 2002, A preliminary experimental study of turbidite fan deposits: Journal of Sedimentary Research, v. 72, p. 619–628, doi:10.1306/032102720619.

Peakall, J., and E. J. Sumner, 2015, Submarine channel flow processes and deposits: A process-product perspective: Geomorphology, v. 244, p. 95–120, doi:10.1016/j.geomorph.2015.03.005.

Pickering, K. T., and J. Corregidor, 2005, Mass-transport complexes (MTCs) and tectonic control on basin-floor submarine fans, middle Eocene, south Spanish Pyrenees: Journal of Sedimentary Research, v. 75, p. 761–783, doi:10.2110/jsr.2005.062.

Pirmez, C., R. T. Beaubouef, S. J . Friedmann, and D. C. Mohrig, 2000, Equilibrium profile and base level in submarine channels: Examples from late Pleistocene systems and implications for the architecture of deep-water reservoirs, *in* P. Weimer, R. M. Slatt, J. Coleman, N. C. Rosen, H. Nelson, A. H. Bouma, M. J. Styzen, and

D. T. Laurence, eds., Deep-water reservoirs of the world: Gulf Coast Section SEPM 20th Annual Research Conference, Houston, Texas, December 3–6, 2000, p. 782–805.
Pirmez, C., R. N. Hiscott, and J. D. Kronen, 1997, Sandy turbidite successions at the base of channel-levee systems of the Amazon fan revealed by FMS logs and cores: Unraveling the facies architecture of large submarine fans, *in* R. Flood, D. J. W. Piper, A. Klaus, and L. C. Peterson, eds., Proceedings of the Ocean Drilling Program, Scientific Results 155, College Station, Texas, Ocean Drilling Program, p. 7–33.
Posamentier, H. W., 2003, Depositional elements associated with a basin floor channel-levee system: Case study from the Gulf of Mexico: Marine and Petroleum Geology, v. 20, p. 677–690, doi:10.1016/j.marpetgeo.2003.01.002.
Posamentier, H. W., and V. Kolla, 2003, Seismic geomorphology and stratigraphy of depositional elements in deep-water settings: Journal of Sedimentary Research, v. 73, p. 367–388, doi:10.1306/111302730367.
Prélat, A., J. A. Covault, D. M. Hodgson, A. Fildani, and S. Flint, 2010, Intrinsic controls on the range of volumes, morphologies, and dimensions of submarine lobes: Sedimentary Geology, v. 232, p. 66–76, doi:10.1016/j.sedgeo.2010.09.010.
Pringle, J. K., R. L. Brunt, D. M. Hodgson, and S. S. Flint, 2010, Capturing stratigraphic and sedimentological complexity from submarine channel complex outcrops to digital 3D models, Karoo Basin, South Africa: Petroleum Geoscience, v. 16, p. 307–330, doi:10.1144/1354-079309-028.
Pyles, D. R., 2008, Multiscale stratigraphic analysis of a structurally confined submarine fan: Carboniferous Ross Sandstone, Ireland: AAPG Bulletin, v. 92, no. 5, p. 557–587, doi:10.1306/01110807042.
Pyles, D. R., D. C. Jennette, M. Tomasso, R. T. Beaubouef, and C. Rossen, 2010, Concepts learned from a 3D outcrop of a sinuous slope channel complex: Beacon channel complex, Brushy Canyon Formation, west Texas, U.S.A.: Journal of Sedimentary Research, v. 80, p. 67–96, doi:10.2110/jsr.2010.009.
Pyles, D. R., L. J. Strachan, and D. C. Jennette, 2014, Lateral juxtapositions of channel and lobe elements in distributive submarine fans: Three-dimensional outcrop study of the Ross Sandstone and geometric model: Geosphere, v. 10, p. 1104–1122, doi:10.1130/GES01042.1.
Schwenk, T., V. Spieß, M. Breitzke, and C. Hübscher, 2005, The architecture and evolution of the Middle Bengal Fan in vicinity of the active channel–levee system imaged by high-resolution seismic data: Marine and Petroleum Geology, v. 22, p. 637–656, doi:10.1016/j.marpetgeo.2005.01.007.
Shepard, F. P., 1948, Submarine geology: New York, Harper and Brothers, 388 p.
Shepard, F. P., 1981, Submarine canyons: Multiple causes and long-time persistence: AAPG Bulletin, v. 65, no. 6, p. 1062–1077.
Shepard, F. P., and K. O. Emery, 1941, Submarine topography off the California coast: Canyons and tectonic interpretation: Boulder, Colorado, Geological Society of America Special Paper 31, 171 p.
Sixsmith, P. J., S. S. Flint, H. D. Wickens, and S. D. Johnson, 2004, Anatomy and stratigraphic development of a basin floor turbidite system in the Laingsburg Formation, Main Karoo Basin, South Africa: Journal of Sedimentary Research, v. 74, p. 239–254, doi:10.1306/082903740239.
Sprague, A. R., M. D. Sullivan, K. M. Campion, G. N. Jensen, F. J. Goulding, D. K. Sickafoose, and D. C. Jennette, 2002, The physical stratigraphy of deep-water strata: A hierarchical approach to the analysis of genetically related stratigraphic elements for improved reservoir prediction, (abs.): AAPG Annual Meeting Abstracts, Houston, Texas, March 10–13, 2002, accessed August 29, 2016, http://www.searchanddiscovery.com/pdfz/abstracts/pdf/2002/annual/SHORT/ndx_41753.pdf.html.
Stevenson, C. J., C. A. L. Jackson, D. M. Hodgson, S. M. Hubbard, and J. T. Eggenhuisen, 2015, Deep-water sediment bypass: Journal of Sedimentary Research, v. 85, p. 1058–1081, doi:10.2110/jsr.2015.63.
Tankard, A., H. Welsink, P. Aukes, R. Newton, and E. Stettler, 2009, Tectonic evolution of the Cape and Karoo basins of South Africa: Marine and Petroleum Geology, v. 26, p. 1379–1412, doi:10.1016/j.marpetgeo.2009.01.022.
Terlaky, V., J. Rocheleau, and R. W. C. Arnott, 2016, Stratal composition and stratigraphic organization of stratal elements in an ancient deep-marine basin-floor succession, Neoproterozoic Windermere Supergroup, British Columbia, Canada: Sedimentology, v. 63, p. 136–135, doi:10.1111/sed.12222.
Torres, J., L. Droz, B. Savoye, E. Terentieva, P. Cochonat, N. H. Kenyon, and M. Canals, 1997, Deep-sea avulsion and morphosedimentary evolution of the Rhône Fan Valley and Neofan during the Late Quaternary (northwestern Mediterranean Sea): Sedimentology, v. 44, p. 457–477, doi:10.1046/j.1365-3091.1997.d01-36.x.
van der Merwe, W. C., S. S. Flint, and D. M. Hodgson, 2010, Sequence stratigraphy of an argillaceous, deepwater basin-plain succession: Vischkuil Formation (Permian), Karoo Basin, South Africa: Marine and Petroleum Geology, v. 27, p. 321–333, doi:10.1016/j.marpetgeo.2009.10.007.
van der Merwe, W. C., D. M. Hodgson, R. L. Brunt, and S. Flint, 2014, Depositional architecture of sand-attached and sand-detached channel-lobe transition zones on an exhumed stepped slope mapped over a 2500 km^2 area: Geosphere, v. 10, p. 1076–1093, doi:10.1130/GES01035.1.
van der Merwe, W. C., D. M. Hodgson, and S. S. Flint, 2009, Widespread syn-sedimentary deformation on a muddy deep-water basin-floor: The Vischkuil Formation (Permian), Karoo Basin, South Africa: Basin Research, v. 21, p. 389–406, doi:10.1111/j.1365-2117.2009.00396.x.
Veevers, J. J., D. I. Cole, and E. J. Cowan, 1994, Southern Africa: Karoo Basin and Cape Fold Belt, *in* J. J. Veevers and A. C. Powell, eds., Permian-Triassic Pangean basins and fold belts along the Panthalassan Margin of Gondwanaland: Geological Society of America Memoir 184, p. 223–279, doi:10.1130/MEM184-p223.
Visser, J. N. J., and H. E. Praekelt, 1996, Subduction, megashear systems and Late Palaeozoic basin development in the African segment of Gondwana: Geologische Rundschau, v. 85, p. 632–646, doi:10.1007/BF02440101.